Manuscript Number:

Title: Performance analysis and optimization of a combined cooling and power system using low boiling point working fluid driven by engine waste heat

Article Type: Original research paper

Section/Category: 1. Energy Conservation and Efficient Utilization

Keywords: Internal combustion engine; Brayton cycle; Waste heat recovery; Dual-pressure organic Rankine cycle; Ejector refrigeration cycle; Optimization

Corresponding Author: Dr. Jiangfeng Wang, Ph.D.

Corresponding Author's Institution: Xi'an Jiaotong University

First Author: Wenge Huang

Order of Authors: Wenge Huang; Jiangfeng Wang, Ph.D.; Jiaxi Xia; Pan Zhao, Ph.D.; Yiping Dai

Abstract: This paper develops a combined cooling and power system to recover waste heat from exhaust gas and jacket water in internal combustion engines using low boiling point fluid as working fluid. The system consists of a CO_2 Brayton cycle (CBC), a dual-pressure organic Rankine cycle (DORC) and an ejector refrigeration cycle (ERC). Comprehensive thermodynamic and exergoeconomic models of the system are performed and seven key parameters are selected to analyze the system performance. To obtain a better performance of the system, single-objective optimization is carried out by means of genetic algorithm with system product levelized exergy cost as the objective function. Results show that the increase of the BC turbine inlet temperature and inlet pressure can cause the increase of the system net power output. In both the high-pressure side and low-pressure side of the DORC, the increase of the ORC turbine inlet temperature causes the increase of the levelized exergy cost while the increase of the ORC turbine inlet pressure does the opposite. The increase of the ejector primary inlet pressure causes the increase of system capital cost. Optimization shows that minimum levelized exergy cost for system product is 53.25 $ $(MWh)^{-1}$ with exergy efficiency of 37.31%.

Suggested Reviewers: Kamel Hooman
University of Qeensland
k.hooman@uq.edu.au

Weifeng He
wfhe@nuaa.edu.cn

Zhixin Sun
zxsun@fzu.edu.cn

Dear Editor:

We are sending a manuscript entitled "Performance analysis and optimization of a combined cooling and power system using low boiling point working fluid driven by engine waste heat", which we should like to submit for publication in Energy Conversion and Management. We investigate a combined cooling and power system driven by exhaust gas and jacket water from an internal combustion engine. The mathematical model of the system is established to simulate the cycles under steady-state conditions. A parametric analysis of seven key parameters is conducted to examine their effects on the thermodynamic and exergoeconomic performance of the system. An optimization is conducted by genetic algorithm to obtain better system performance.

We declare that the manuscript has not been previously published, is not currently submitted for review to any other journal and will not be submitted elsewhere before one decision is made. Its publication is approved by all authors. If accepted, it will not be published elsewhere in the same form, in English or in any other language.

We appreciate your consideration of our manuscript, and we look forward to receiving comments from the reviewers.

Sincerely,

Jiangfeng Wang (on behalf of the authors' team)

Institute of Turbomachinery

Cover letter

Shaanxi Engineering Laboratory of Turbomachinery and Power Equipment

State Key Laboratory of Multiphase Flow in Power Engineering

School of Energy and Power Engineering

Xi'an Jiaotong University, Xi'an, China

Highlights

A combined cooling and power system driven by engine exhaust gas and jacket water is proposed.

Thermodynamic and exergoeconomic performance of the system are analyzed.

Optimization for the combined cooling and power system is conducted by genetic algorithm.

1 **Performance analysis and optimization of a combined**

2 **cooling and power system using low boiling point working**

3 **fluid driven by engine waste heat**

4 Wenge Huang, Jiangfeng Wang*, Jiaxi Xia, Pan Zhao, Yiping Dai

5 Institute of Turbomachinery, Shaanxi Engineering Laboratory of Turbomachinery and

6 Power Equipment, State Key Laboratory of Multiphase Flow in Power Engineering,

7 School of Energy and Power Engineering, Xi'an Jiaotong University, Xi'an 710049,

8 China

9 **Corresponding author:** Jiangfeng Wang

10 **Mailing address:**

11 Institute of Turbomachinery, Shaanxi Engineering Laboratory of Turbomachinery and

12 Power Equipment, State Key Laboratory of Multiphase Flow in Power Engineering,

13 School of Energy and Power Engineering

14 Xi'an Jiaotong University, Xi'an 710049, China

15 E-mail address: jfwang@mail.xjtu.edu.cn (JF Wang).

16

17 **Performance analysis and optimization of a combined**

18 **cooling and power system using low boiling point working**

19 **fluid driven by engine waste heat**

20 Wenge Huang, Jiangfeng Wang*, Jiaxi Xia, Pan Zhao, Yiping Dai

21 Institute of Turbomachinery, Shaanxi Engineering Laboratory of Turbomachinery and

22 Power Equipment, State Key Laboratory of Multiphase Flow in Power Engineering,

23 School of Energy and Power Engineering, Xi'an Jiaotong University, Xi'an 710049,

24 China

25 **Abstract**

26 This paper develops a combined cooling and power system to recover waste heat

27 from exhaust gas and jacket water in internal combustion engines using low boiling

28 point fluid as working fluid. The system consists of a CO_2 Brayton cycle (CBC), a

29 dual-pressure organic Rankine cycle (DORC) and an ejector refrigeration cycle (ERC).

30 Comprehensive thermodynamic and exergoeconomic models of the system are

31 performed and seven key parameters are selected to analyze the system performance.

32 To obtain a better performance of the system, single-objective optimization is carried

33 out by means of genetic algorithm with system product levelized exergy cost as the

34 objective function. Results show that the increase of the BC turbine inlet temperature

35 and inlet pressure can cause the increase of the system net power output. In both the

36 high-pressure side and low-pressure side of the DORC, the increase of the ORC

37 turbine inlet temperature causes the increase of the levelized exergy cost while the

38 increase of the ORC turbine inlet pressure does the opposite. The increase of the

39 ejector primary inlet pressure causes the increase of system capital cost. Optimization

40 shows that minimum levelized exergy cost for system product is 53.25 $ $(MWh)^{-1}$

41 with exergy efficiency of 37.31%.

42 Keyworks:

43 Internal combustion engine

44 Brayton cycle

45 Waste heat recovery

46 Dual-pressure organic Rankine cycle

47 Ejector refrigeration cycle

48 Optimization

49 **Nomenclature**

A	area, m^2		ρ	density, kg m^{-3}
BC	Brayton cycle		μ	dynamic viscosity, m^2 s^{-1}
B_o	boiling number		η	efficiency, %
c	average cost per unit of exergy, $ $(MWh)^{-1}$		δ	thickness, m
c_p	specific heat, kJ kg^{-1} K^{-1}		*Subscribe*	
C	cost rate, $ year^{-1}		1-31	state points
CBC	CO$_2$ Brayton cycle		g1-g3	state points
CCP	combined cooling and power		w1-w3	state points
CRF	capital recovery factor		Bt	Brayton cycle turbine
$CEPCI$	chemical engineering plant cost index		BM	bare module
D	diameter, m		cond	condenser

DORC	dual-pressure organic Rankine cycle	comp	compressor
e	exergy, kJ kg^{-1}	D	destruction
E	exergy flow rate, kJ s^{-1}	elec	electricity
E_y	exergy flow rate per year, kJ year^{-1}	es	equivalent diameter
ERC	ejector refrigeration cycle	ev	evaporation/evaporator
F	multiplying factor	ex	exergy
f	friction factor	F	fuel
G	mass flow rate, kg s^{-1}	g	exhaust gas
h	enthalpy, kJ kg^{-1}	gh	gas heater
H	depth, m	he	heat exchanger
i_{eff}	interest rate	L	loss
l	length, m	l	liquid
M	mass flow rate, kg s^{-1}	M	material
n	lifetime, year	Ot	ORC turbine
Nu	Nusselt number	P	product
P	pressure, MPa	p1	pump 1
Pr	Prandtl number	p2	pump 2
Pt	center distance between tubes, m	p3	pump 3
P_r	reduced pressure	p4	pump 4
Q	heat transfer rate, kW	pf	primary flow
Q_{cool}	cooling capacity, kW	prec	precooler
q_{m}	average imposed wall heat flux, W m^{-2}	preh	preheater

r_f	enthalpy of vaporization, kJ kg^{-1}	s	shell
T	temperature, K	t	tube
U	overall heat transfer coefficient, W m^{-2} K^{-1}	th	thermal
W	power, kW	turb	turbine
W_y	annually power, MWh year^{-1}	vg	vapor generator
x	vapor quality	w	tube wall
Z	annually levelized cost value, $ year^{-1}		
z	capital cost, K$		
Greek symbol			
α	convection heat transfer coefficient, W m^{-2} K^{-1}		
λ	heat conductivity, W m^{-1} K^{-1}		

1. Introduction

50

51   Nowadays, internal combustion engines (ICEs) are the major motive power source

52   in energy field. ICEs are used widely in transport, construction, agriculture, etc. Over

53   50% of the total transportation fuel is consumed by internal combustion engines. In a

54   typical ICE, only 30-45% of the fuel energy is converted into effective power output,

55   while the remaining energy is discharged to environment via exhaust gas, jacket water

56   and other means, including charge air and lubrication [1]. Thus, technologies utilizing

57   waste heat from ICEs have been investigated by a number of researchers.

58   Compared to other methods, organic Rankine cycle (ORC) is recognized as a well

59   proven and highly efficient waste heat recovery technology [2,3]. Coupling the ORC

60   with the internal combustion engines is getting increasing interest of researchers. A

61   volume of work was conducted to examine the potential of waste heat recovery from

62   ICE with the help of ORC. Kalyan et al. [4] designed a system using ORC to generate

63   power from exhaust gas in a low temperature combustion engine. Wei et al. [5]

64   integrated an ORC system with a heavy-duty diesel engine to recover the waste heat.

65   Srinivasan et al. [6] designed an ORC waste heat recovery system to improve the

66   efficiency of the gas engine. Tian et al. [7] designed an ORC power generation system

67   using engine exhaust gas as heat source.

68   Attention was mainly focused on the exhaust gas when people explored waste heat

69   recovery from ICEs at early stage. ORC-based waste recovery systems mentioned

70   above only absorbed heat from engine exhaust gas. However, there is a large amount

71   energy exists in engine jacket water for its large mass flow rate and relatively high

72   temperature (about 90℃). ORC-based power generation systems absorbed heat both

73   form exhaust gas and jacket water were introduced by researchers. Vaja and

74   Gambarotta [8] examined three different ORC cycles including a simply cycle, a

75   preheating cycle and a regenerative cycle. Cycle preheated by jacket water was able to

76   increase the system efficiency by about 12.5%. Rosset et al. [9] compared different

77   ORC cycle configurations which converted waste heat from exhaust gas, from jacket

78   water and from both. Calculation results revealed that the dual-source cycle provided

79   the highest net power output.

80   To achieve a better performance for the waste heat recovery system, many studies

81   try to improve the configurations of ORCs. Zhang et al. [10] developed a novel

82   system driven by waste heat in an ICE with a dual-loop ORC. The high-temperature

83   cycle absorbed heat from the exhaust gas and the low-temperature cycle recovered

84   heat from the high-temperature cycle and the jacket water. Yang et al. [11] modeled a

85   dual-loop ORC system driven by waste heat in ICE. High-temperature cycle absorbed

86   heat from the exhaust gas and low-temperature cycle absorbed heat from secondary

87   exhaust gas and the jacket water. Ge et al. [12] designed a dual-loop ORC system to

88   recover waste heat using different working fluids. Zeotropic mixture was used to

89   recover high-temperature exhaust gas and R600a/R601a mixture was used to absorb

90   heat in low-temperature jacket water. Systems integrated with complicated organic

91   Rankine cycles were developed by many researchers [13-15].

92   Thermal stability of the organic working fluid should be considered when developing

93   organic Rankine cycles to recovery waste heat from engine exhaust gas.

94   Organic-based fluids would decompose under high-temperature and high-pressure

95   conditions [16]. The low decomposition temperature of organic working fluid in ORC

96   is about 200-300℃ while the temperature of engine exhaust gas can be more than

97   500℃. For all the studies mentioned above, the organic working fluid absorbs heat

98   directly form the high-temperature exhaust gas, causing the potential of working fluid

99   decomposition. Though an intermediate loop with thermal oil can be added between

100   the ORC and the exhaust gas to avoid the decomposition [17,18], a large amount of

101   high-temperature waste heat is not utilized at all. In order to solve this issue,

102   researchers placed other waste heat recovery system between the ORC and exhaust

103   gas to exploit to high-temperature waste heat. Thermoelectric generator (TEG), for

104   example, was introduced by Miller et al. [19] to the utilize the high temperature waste

105   heat in exhaust gas. After the TEG process, the cooled exhaust gas could drive the

106   ORC safely. However, because of the low energy conversion capacity of the TEG,

107   power generated by the TEG was much smaller than the ORC in the same system [20].

108   Shu et al. [21] placed a steam Rankine cycle between ORC and exhaust gas for waste

109   heat recovery from the gas engines. The steam Rankine cycle was the topping cycle to

110   recovery heat from the high-temperature exhaust gas and organic Rankine cycle was

111   the bottoming cycle to recovery heat from the exhaust water vapor. Large power

112   output was provided by both the steam Rankine cycle and the ORC in the system.

113   However, steam in the steam Rankine cycle requires a large superheated degree, or it

114   may condense during the expansion and damage the turbine blades. As a result,

115   structure of the steam Rankine cycle turbine is complex. Brayton cycle (BC), on the

116   contrary, presents the advantages of simple and reliable structure. It uses gas as

117   working fluid which does not involve phase change during the expansion [22]. Thus,

118   Brayton-ORC systems can be used to exploit the waste heat from ICE effectively and

119   safely.

120   Quite a few studies have been published to improve the waste heat recovery from

121   exhaust gas. Jacket water, though explored by some researchers, is mainly used as the

122   low-temperature heat source to preheat the organic working fluid in ORC. However,

123   the mismatching mass flow rate of organic working fluid in the preheater and the

124   evaporator causes a large amount of heat waste in jacket water. Yu et al. [23]

125   calculated the energy recovery efficiency from an ORC- based ICE waste heat

126   recovery system. 75% waste heat could be recovered from exhaust gas while 9.5%

127   waste heat was recovered from jacket water. But for most ICEs (rated power between

128   500 kW and 2000 kW), discharged thermal energy in jacket water is approximately

129   the same as the energy in exhaust gas [24]. Thus, a large amount of waste heat in

130   jacket water is potentially valuable for recovery.

131   Usually, traditional power plants only generate power and can't fulfill the

132   requirements of the consumers for energy supply. Cooling capacity, for example, is

133   needed in many places such as hospital, hotel, restaurant, etc. To satisfy the various

134   demands of the consumers and to recover the waste heat more efficiently,

135   cogeneration systems is introduced by many researchers. Cogeneration systems driven

136   by waste heat in internal combustion engines were developed by a number of

137   investigators. Chen et al. [25] designed an ammonia-water combined cooling and

138   power system using the waste heat from the ICEs. Ammonia-water was heated by

139   exhaust gas and jacket water. One part of the ammonia-water vapor flew into the

140   turbine to provide power and the other part flew into the evaporator to provide

141   refrigeration. Salek et al. [26] coupled an ammonia absorption refrigeration cycle and

142   a bottoming Rankine cycle with internal combustion engine to produce power and

143   cooling capacity. Absorption refrigeration cycles were considered by most of the

144   combined cooling and power systems to convert exhaust gas waste heat to cooling

145   capacity. However, ejector refrigeration cycle, which presents the advantages of

146   desirable efficiency, small structure and simple layout [27,28], is always neglected.

147   In this study, a combined cooling and power system is developed, which comprises

148   a CO_2 Brayton cycle, a dual-pressure ORC and an ejector refrigeration cycle. The

149   CO_2 Brayton cycle is used to recover the waste heat from high-temperature exhaust

150   gas directly. The turbine exhaust in the CO_2 Brayton cycle and the engine exhaust gas

151   after heat transfer are respectively regarded as the heat sources for the high-pressure

152   side and low-pressure side of the dual-pressure ORC, realizing the cascading

153   utilization of exhaust gas waste heat. Meanwhile, organic working fluid in

154   high-pressure side and low-pressure side are both preheated by jacket water to make

155   full use of the waste heat. What's more, the ejector refrigeration cycle is adapted to

156   recover the waste heat of jacket water further and produce cooling capacity

157   simultaneously. Thermodynamic and exergoeconomic analysis is carried out to

158   examine the effects of key parameters on system performances. Then a system

159   optimization is conducted to obtain the minimum levelized exergy cost for the system

160   product by means of genetic algorithm.

161   **2. System description**

162   2.1.   CCP system

163   The combined cooling and power (CCP) system is shown in Fig 1. The system

164   integrates a dual-pressure organic Rankine cycle with a CO_2 Brayton cycle and an

165   ejector refrigeration, which can produce power and cooling capacity simultaneously.

166   The exhaust gas from the internal consumption engine enters the gas heater to drive

167   the CO_2 Brayton cycle. CO_2 cooled by the precooler flows through the compressor to

168   be compressed to a supercritical state. Then the high-pressure CO_2 absorbs heat in the

169 gas heater, becoming high-pressure and high-temperature state, and enters BC turbine

170 to produce power.

171   After expanding in the BC turbine, the high-temperature exhaust CO_2 flows into

172 vapor generator 2 to heat the organic working fluid. High-pressure side organic

173 working fluid heated by the CO_2 then flows into the ORC turbine to produce power.

174 Meanwhile low-pressure side organic working fluid absorbs heat from the secondary

175 engine exhaust gas in vapor generator 1 and then enters ORC turbine to produce

176 power.

177   Exhaust vapor from the ORC turbine is cooled by condenser 1 to liquid state and

178 pressured by pump 1. Jacket water with large mass flow rate is used to preheat the

179 organic working fluid in the preheater. The preheated organic working fluid then

180 separates. One part of the fluid is pumped by pump 3 to the vapor generator 1 to cycle

181 in the low-pressure side. The other part is pumped by pump 2 to the vapor generator 2

182 to cycle in the high-pressure side.

183   The jacket water then flows into vapor generator 3 to provide heat for the ejector

184 refrigeration cycle. After the condensation process in condenser 2, liquid working

185 fluid is divided into two separated parts. One part of the fluid is pumped to the vapor

186 generator 3 to absorb heat from jacket water and then becomes superheated vapor.

187 The other part of the working fluid flows through the throttle valve to become

188 low-pressure vapor-liquid mixture. The low-pressure mixture enters the evaporator to

189 produce cooling capacity when absorbing heat from the environment and become

190 low-pressure vapor. After that, the superheated vapor mixes with the low-pressure

191   vapor in the ejector. The mixed working fluid enters the condenser 2 to be condensed

192   to liquid.

193   R245fa is selected as the working fluid for the organic Rankine cycle and the

194   ejector refrigeration cycle because of the great thermodynamic performance and the

195   low environment effect [29,30].

196   **3. System model**

197   Several assumptions are made to simplify the simulation of the system.

198   (1) The system keeps a steady state.

199   (2) The heat and friction losses in the system are not considered.

200   (3) The pressure losses in the vapor generator, preheater, precooler, evaporator and

201   condenser are neglected.

202   (4) Considering the low gas acid dew point temperature, the gas temperature at the

203   outlet of the vapor generator 1 is higher than 110℃ [31].

204   (5) The working fluid out of the condensers and preheater is saturated liquid and the

205   state at the outlet of the evaporator is saturated vapor.

206   (6) The process through the throttle valve is isenthalpic.

207   3.1.   Thermodynamic model

208   3.1.1.   Energy model

209   The net power of the CO_2 Brayton cycle is expressed as:

210    $W_{BC} = W_{Bt} - W_{comp}$ (1)

211   The net power of the DORC is given as:

212    $W_{\text{ORC}} = W_{\text{Ot}} - W_{\text{p1}} - W_{\text{p2}} - W_{\text{p3}}$ (2)

213   The cooling capacity of the ERC is given as:

214    $Q_{\text{cool}} = M_{\text{cool}} \cdot (h_{21} - h_{20})$ (3)

215   The net power output of the whole system is calculated as:

216    $W_{\text{net}} = W_{\text{ORC}} + W_{\text{BC}} - W_{\text{p4}}$ (4)

217   The thermal efficiency of the system is given as:

218    $\eta_{\text{th}} = \dfrac{W_{\text{net}} + Q_{\text{cool}}}{M_{\text{g1}} \cdot (h_{\text{g1}} - h_{\text{g3}}) + M_{\text{w1}} \cdot (h_{\text{w1}} - h_{\text{w3}})}$ (5)

219   The detailed energy model equations of each component are list in Table 1. Note

220   that there are two expanding processes in the ORC turbine. The high-pressure side

221   vapor expands from high pressure (state 10) to low pressure (state 11) for the first

222   time and then mixes with the low-pressure side vapor. After that, the mixed vapor

223   expands from low pressure (state 11) to the back pressure of ORC turbine (state 12)

224   for the secondary time.

225   3.1.2.   Exergy model

226   In general, the energy model of a system is based on the first law of the

227   thermodynamic which focuses the amount of the thermal energy in the system. The

228   exergy model of the system is based on the second law of the thermodynamic which

229   focuses on the quality of the thermal energy. The exergy analysis of the system is

230   based on a dead state (the ambient conditions in this paper). The equation of exergy

231   for unit working fluid is expressed as:

232 $e = (h - h_0) - T_0 \cdot (s - s_0)$ (6)

233 where h_0, T_0 and s_0 are the parameters under the ambient conditions.

234 The exergy flow rate in this study is given by:

235 $E = M \cdot e$ (7)

236 All the components in the system are associated directly or indirectly with fuel or

237 other heat sources, such as exhaust gas and jacket water in this study. The heat sources

238 provide exergy for the components to operate. For each component, there is an exergy

239 balance equation, being expressed as [32]:

240 $E_F = E_P + E_D + E_L$ (8)

241 where E_F is the rate of exergy for the component fuel and E_P represents the rate of

242 exergy for the component product; E_D denotes the rate of component exergy

243 destruction and E_L expresses the rate of exergy loss for the component.

244 The details of the exergy balance equations for each component are listed in Table

245 1.

246 The exergy efficiency represents the degree of the utilization of the waste heat in

247 the system, being expressed as:

248 $\eta_{ex} = \dfrac{W_{net} + E_{cool}}{E_{g1} - E_{g3} + E_{w1} - E_{w3}}$ (9)

249 where E_{cool} is the exergy rate of the cooling process, being expressed as:

250 $E_{cool} = E_{25} - E_{24}$ (10)

251   3.2.   Capital cost and exergoeconomic model of the system

252   3.2.1.   Capital cost calculation

253   In this study, a method of modeling the capital costs of the main component is

254   employed [33]. At first, the bare module cost of the components is calculated as the

255   basic cost. The basic cost of the components includes the direct project cost (such as

256   equipment cost, material cost for the installation, etc.) and the indirect project cost

257   (like the taxes, insurance engineering expenses etc.). The bare module cost of the

258   components is calculated under basic conditions. For conditions different from the

259   basic conditions, multiplying factors (the specific equipment type, the specific system

260   pressure and the specific material of construction) are added in the calculation to

261   correct the results.

262   Axial turbines (BC turbine and ORC turbine) are used in this study. The bare

263   module cost equation of the turbine is:

264    $$\log_{10} C^0_{turb} = K_{1,turb} + K_{2,turb} \cdot \log_{10} W + K_{3,turb} \cdot (\log_{10} W)^2 \tag{11}$$

265   where K_{turb} is constant corresponding to the turbine type; W is the power output of the

266   turbine.

267   Turbines used in this study are made of carbon steel (CS) and operate under high

268   pressure. Thus, a multiplying factor is used to correct the result. The capital cost of the

269   turbine is given as:

270    $$C_{turb} = F_{BM,turb} \cdot C^0_{turb} \tag{12}$$

271   where $F_{BM,turb}$ is the multiplying factor corresponding to the working conditions of the

272   turbine.

273   Reciprocating pumps are used in this study. The bare module cost equation of the

274   pumps is given as:

275    $$\log_{10} C_{pump}^0 = K_{1,pump} + K_{2,pump} \cdot \log_{10} W + K_{3,pump} \cdot (\log_{10} W)^2 \tag{13}$$

276   where K_{pump} is constant corresponding to the pump type; W is the power input of the

277   pump.

278   Pumps used in this study are made of stainless steel (SS) and work under high

279   pressure. Thus, multiplying factors are used to correct the bare module cost. The

280   capital cost of the pump is given as:

281    $$C_{pump} = \left(B_{1,pump} + B_{2,pump} \cdot F_{M,pump} \cdot F_{P,pump} \right) \cdot C_{pump}^0 \tag{14}$$

282   where B_{pump} is constant corresponding to the type of the pump; $F_{M,pump}$ is the material

283   factor of the pump and $F_{P,pump}$ is the pressure factor of the pump. The equation of the

284   pressure factor is given as:

285    $$\log_{10} F_{P,pump} = C_{1,pump} + C_{2,pump} \cdot \log_{10} P_{pump} + C_{3,pump} \cdot (\log_{10} P_{pump})^2 \tag{15}$$

286   where C_{pump} is the constant corresponding to the type of the pump and P_{pump} is the

287   pressure of the pump under working conditions.

288   Axial compressor is used in this study. The bare module cost equation of the

289   compressor is given as:

290    $$\log_{10} C_{comp}^0 = K_{1,comp} + K_{2,comp} \cdot \log_{10} W + K_{3,comp} \cdot (\log_{10} W)^2 \tag{16}$$

291   where K_{comp} is the constant corresponding to the type of the compressor; W is the

292   power input of the compressor.

293   The compressor is made of carbon steel (CS) and works under high pressure.

294   Correction equation of the bare module cost is given as:

295 $$C_{\text{comp}} = F_{\text{BM,comp}} \cdot C_{\text{comp}}^{0} \tag{17}$$

296 where $F_{\text{BM,comp}}$ is the constant corresponding to the type of the compressor.

297 Tube-and-shell heat exchangers (gas heater, vapor generators, precooler, preheater,

298 evaporator and condensers) are used in this study. The bare module cost equation of

299 the heat exchanger is given as:

300 $$\log_{10} C_{\text{he}}^{0} = K_{1,\text{he}} + K_{2,\text{he}} \cdot \log_{10} A + K_{3,\text{he}} \cdot (\log_{10} A)^{2} \tag{18}$$

301 where K_{he} is the constant corresponding to the type of the heat exchanger; A is the

302 heat transfer area of the heat exchanger. The calculation of the heat exchanger areas is

303 presented in Appendix A.

304 Heat exchangers used in this study are made of carbon steel (CS) and work under

305 different pressure. Multiplying factors are needed to correct the results, the equation is

306 given as:

307 $$C_{\text{he}} = \left(B_{1,\text{he}} + B_{2,\text{he}} \cdot F_{\text{M,he}} \cdot F_{\text{P,he}} \right) \cdot C_{\text{he}}^{0} \tag{19}$$

308 where B_{he} are the constants correspond to the type of the heat exchanger. $F_{\text{M,he}}$ and

309 $F_{\text{P,he}}$ are the material factor and pressure factor, respectively. The pressure factor is

310 obtained from the following equation:

311 $$\log_{10} F_{\text{P,he}} = C_{1,\text{he}} + C_{2,\text{he}} \cdot \log_{10} P_{\text{he}} + C_{3,\text{he}} \cdot (\log_{10} P_{\text{he}})^{2} \tag{20}$$

312 where C_{he} is the constant corresponding to the type of the heat exchanger; P_{he} is the

313 designed working pressure for the heat exchanger.

314 The values of the constants mentioned above for the main components are listed in

315 Appendix B.

316   The calculation of the bare module cost depends on past records or published

317   correlations for price information. It is necessary to update the costs because of the

318   changing economic conditions (inflation). This can be achieved by the following

319   expression:

320    $$C_2 = C_1 \cdot \left(\frac{I_2}{I_1} \right)$$ (21)

321   where C is the purchased cost and I is the cost index. The subscript 1 refers to base

322   time when cost is known and subscript 2 refers to time when cost is desired. The

323   *CEPCI* (Chemical Engineering Plant Cost Index) is employed to calculate the

324   inflation. The values of $CEPCI_{2016}$ and $CEPCI_{ref,2001}$ are 541.7 and 397, respectively

325   [34,35].

326   3.2.2.   Exergoeconomic model

327   Exergoeconomic is a branch of engineering which combines the thermodynamic

328   analysis and economic principles. Thermodynamic performance and economic cost of

329   the system are all taken into consideration.

330   To find the relationship between the present value of the expenditure and the

331   equivalent annually levelized costs, the capital recovery factor (CRF) is employed,

332   being expressed as [32]:

333    $$Z_i = CRF \cdot C_i$$ (22)

334    $$CRF = \frac{i_{eff} \cdot (1 + i_{eff})^n}{(1 + i_{eff})^n - 1}$$ (23)

335   where i_{eff} is the effective discount rate with a value of 0.05 [36]; n is the lifetime of the

336   CCP system being assumed as 30 [37].

337   In order to calculate the equivalent annually levelized costs, the annual working

338   time of the system is assumed as 8000 h [38]. Then the annual exergy rates and annual

339   power output or consumption are obtained.

340   In a steady system, there are a number of entering and outing working fluid steams

341   and heat and work interactions with the surroundings. In exergoeconomic analysis,

342   each flowing steam is associated with a levelized exergy cost. The equations to

343   calculate the cost of the steam product are given as:

344     $C_{in} = c_{in} \cdot E_{y,in}$ (24)

345     $C_{out} = c_{out} \cdot E_{y,out}$ (25)

346     $C_{work} = c_{work} \cdot W_y$ (26)

347     $C_{heat} = c_{heat} \cdot E_{y,heat}$ (27)

348   where c denotes levelized exergy cost of the steams; $E_{y,in}$ and $E_{y,out}$ are the exergy

349   transfer rate of the steam flowing in and out a component; W_y and $E_{y,heat}$ are the power

350   and the heat transfer rate of the components considering the annual working time.

351   The cost balance equation applied to the kth system component is given as:

352     $\sum_{out} C_{out,k} + C_{w,k} = C_{heat,k} + \sum_{in} C_{in,k} + Z_k$ (28)

353   Details of the cost balance equation are listed in Table 2.

354   The levelized exergy cost for system product is chosen to indicate the

355   exergoeconomic performance, being expressed as [39,40]:

356     $c_{product} = c_{capital} + c_{fuel}$ (29)

357 where $c_{capital}$ is the capital-cost-related part of the levelized exergy cost for the system

358 product, being expressed as:

359 $$c_{capital} = \frac{Z_{total}}{W_{net} + E_{cool}}$$ (30)

360 c_{fuel} is the fuel-cost-related part of the levelized exergy cost for the system product,

361 being expressed as:

362 $$c_{fuel} = \frac{c_{Bt} \cdot W_{y,comp} + c_{Ot} \cdot W_{y,pump1} + c_{Ot} \cdot W_{y,pump2} + c_{Ot} \cdot W_{y,pump3} + c_{Ot} \cdot W_{y,pump4}}{W_{net} + E_{cool}}$$ (31)

363 c_{Bt} and c_{Ot} are the levelized exergy cost for the BC turbine power output and the

364 ORC turbine power output, which are calculated in Table 3. Likewise, they can be

365 expressed as the capital-cost-related part and the fuel-cost-related part:

366 $$c_{Bt} = \frac{Z_{Bt}}{W_{y,Bt}} + \frac{c_3 \cdot (E_{y,3} - E_{y,4})}{W_{y,Bt}}$$ (32)

367 $$c_{Ot} = \frac{Z_{Ot}}{W_{y,Ot}} + \frac{c_{10} \cdot (E_{y,10} + E_{y,11} - E_{y,12})}{W_{y,Ot}}$$ (33)

368 In addition, the levelized exergy cost for the condensers and the precooler is equal

369 to zero, being given by:

370 $c_{26} = c_{28} = c_{30} = 0$ (34)

371 The levelized exergy cost for the exhaust gas as well as the jacket water is zero,

372 being expressed as:

373 $c_{g1} = c_{w1} = 0$ (35)

374 **4. Results and discussion**

375 4.1.1.   Simulation conditions for the system

376   The thermodynamic parameters of the working fluid are calculated under the

377 environment of MATLAB with the help of REFPROP 9.1 [41]. The basic conditions

378 of simulation for the CCP system are listed in Table 3

379 4.1.2.   Internal combustion engine

380   In this study, the engine selected [8] is a 12-cylinder 4-stroke supercharged gas

381 engine. The main designed parameters of the engine are listed in Table 4. The

382 composition of the engine exhaust gas is presented in Table 5. The heat load capacity

383 of the engine exhaust gas is about 1700 kW when cooled down to the acid dew

384 temperature and the 1000 kW can be obtained from the engine jacket water.

385 4.2.   Analysis for the thermodynamic and exergoeconimic performance

386   Seven key parameters (BC turbine inlet temperature, BC turbine inlet pressure, inlet

387 temperature at the high-pressure side of ORC turbine, inlet pressure at the

388 high-pressure side of ORC turbine, inlet temperature at the low-pressure side of ORC

389 turbine, inlet pressure at the low-pressure side of ORC turbine and the ejector primary

390 inlet pressure) are chosen to analyze the thermodynamic and exergoeconomic

391 performance of the system. In the thermodynamic aspect, the net power output of the

392 CO_2 Brayton cycle (W_{BC}), net power output of the DORC (W_{ORC}), net power of the

393 whole system (W_{net}), cooling capacity of the system (Q_{cool}) and the exergy efficiency

394   of the system (η_{exergy}) are selected to reflect the system performance. Levelized

395   exergy cost for the BC turbine power output (c_{Bt}), levelized exergy cost for the ORC

396   turbine power output (c_{Ot}), levelized exergy cost the system product (c_{product}) and the

397   system capital cost (z_{capital}) are chosen to represent the exergoeconomic performance.

398   4.2.1.   Variations of thermal parameters in CBC

399   The influences of the BC turbine inlet temperature on the output and the exergy

400   efficiency of the system are shown in Fig. 2. The net power output of the CO_2 Brayton

401   cycle (CBC) increases with the rise of the BC turbine inlet temperature. That can be

402   explained by the decrease of the compressor power consumption. With the increase of

403   the CO_2 temperature at the BC turbine inlet, the mass flow rate of CO_2 decreases. As a

404   result, less CO_2 working fluid is compressed by the compressor, leading to the

405   decrease of the compressor power consumption. On the one hand, the decrease of the

406   mass flow rate cuts down the BC turbine power output. On the other hand, the

407   increase of inlet temperature causes the increase of enthalpy drop of CO_2 in the

408   turbine which results in the increase of the BC turbine power output. The two effects

409   mention above cause the slight decrease of the BC turbine power output, which is

410   smaller than the decrease of the compressor power consumption. Thus, the large

411   decrease of the compressor power consumption determines the increase of the CBC

412   net power output.

413   It is presented that the net power output of the DORC increases with the rise of the

414   BC turbine inlet temperature. The temperature of the exhaust CO_2 increases with the

415   increase of BC turbine inlet temperature. Since the exhaust CO_2 acts as the heat

416   source for organic working fluid in the high-pressure side of DORC, more heat is

417   provided in vapor generator 2. As a result, the mass flow rate of the organic working

418   fluid increases, leading to the rise of the power output of the ORC turbine. The

419   increase of the power consumption of the pumps in the DORC is much smaller than

420   the increase of the ORC turbine power output. Thus, the net power output of the

421   DORC increases.

422   The net power of the whole CCP system increases with the increase of the BC

423   turbine inlet temperature. That can be explained by the increase of the CO_2 Brayton

424   cycle net power output and the DORC net power output. The increase of the net

425   power output of the system causes the increase of the exergy efficiency of the system.

426   With the increase of the BC turbine inlet temperature, the cooling capacity of the

427   ejector refrigeration cycle (ERC) decreases, as shown in Fig. 2. As discussed above,

428   the increase of the exhaust CO_2 temperature causes the increase of the organic

429   working fluid mass flow rate in DORC. Thus, more heat is absorbed by the organic

430   working fluid in the preheater from the jacket water. Less heat is available for the

431   ERC working fluid in vapor generator 3. As a result, the mass flow rate of the

432   working fluid in the evaporator decreases, resulting in the decrease of the cooling

433   capacity of the CCP system.

434   The influences of the BC turbine inlet temperature on the levelized exergy cost and

435   the system capital cost of the system are shown in Fig. 3. The levelized exergy cost

436   for the BC turbine power output decreases with the increase of the BC turbine inlet

437 temperature. Since the decrease of the compressor power consumption, the cost of

438 compressor decreases. According to Eq. (32), the decrease of compressor cost leads to

439 the decrease of capital-cost-part of the levelized exergy cost for the BC turbine power

440 output c_{Bt}. Thus, c_{Bt} decreases. The levelized exergy cost for the ORC turbine

441 decreases with the increase of the BC turbine inlet temperature. The reason for this is

442 the large increase of the power output of the ORC turbine. The increase of the ORC

443 turbine power output causes the increase of both the capital-cost-related part and

444 fuel-cost-related part of c_{Ot}.

445 The system capital cost increases with the increase of the BC turbine inlet

446 temperature. Since the large increase of the ORC turbine power output, the cost of the

447 ORC turbine increases. Meanwhile, the increase of the mass flow rate of the organic

448 working fluid in the DORC causes the increase of the cost for the vapor generator 2

449 and preheater. Though the cost of the compressor decreases with the decrease of the

450 compressor power consumption, the effect of the ORC turbine cost is more important,

451 which determines the rise of the system capital cost.

452 It can be obtained in Fig. 3 that the levelized exergy cost for the system product

453 decreases with the increase of the BC turbine inlet temperature. As mentioned above,

454 the levelized exergy cost for the BC turbine and ORC turbine decrease. Analyzing

455 from Eq. (31), the fuel-cost-related part of the levelized exergy cost for system

456 product decreases. According to Eq. (30), the increase of system net power output

457 causes the decrease of the capital-cost-related part of the levelized exergy cost for the

458 system product. As a result, the levelized exergy cost for the system product

459   decreases.

460   The influences of the BC turbine inlet pressure on the output and the exergy

461   efficiency of the system are shown in Fig. 4. The net power output of the CBC

462   increases with the increase of the BC turbine inlet pressure. Since the increase of

463   pressure at BC turbine inlet, the enthalpy drop of the CO_2 in the BC turbine increases,

464   causing the increase of the BC turbine power output. The pressure rise also causes the

465   increase of compressor power consumption. But the increase of the BC turbine power

466   output is larger than the increase of the compressor power consumption. As a result,

467   the net power output of the CBC increases.

468   The net power output of the DORC decreases with the increase of the BC turbine

469   inlet pressure. On the one hand, the temperature of the exhaust CO_2 at the BC turbine

470   outlet decreases with the increase of the BC turbine inlet pressure. Thus, less heat is

471   provided in vapor generator 2, causing the decrease of the mass flow rate of the

472   organic working fluid in the high-pressure side DORC. As a result, the power output

473   of the high-pressure side DORC decreases. On the other hand, the increase of the BC

474   turbine inlet pressure causes the increase of the compressor power consumption which

475   results in the rise of the CO_2 temperature at the compressor outlet. Thus, less heat is

476   absorbed by CO_2 in the gas heater and more heat is transferred to the organic working

477   fluid in vapor generator 1. The mass flow rate of the organic working fluid in the

478   low-pressure side DORC increases, causing the increase of the power output in the

479   low-pressure side. The increase of the power output in low-pressure side is smaller

480   than the decrease of power output in the high-pressure side. Thus, the net power of the

481   whole DORC decreases.

482   The cooling capacity of the system increases with the increase of the BC turbine

483   inlet pressure. The decrease of the mass flow rate in the high-pressure side of DORC

484   is more than the increase of the mass flow rate in the low-pressure side. As a result,

485   the total mass flow in the DORC decreases. Thus, less heat is absorbed from the

486   jacket water in the preheater and more heat is available in vapor generator 3 for

487   working fluid in the ERC. The mass flow rate of the working fluid in ERC increases,

488   causing the increase of the cooling capacity.

489   The net power output of the whole system increases with the increase of the BC

490   turbine inlet pressure. Though the net power output of the DORC decreases, the

491   increase of CBC net power output is much larger than the decrease. As a result, the

492   net power output of the whole system increases. The increase of the net power output

493   of the CCP system causes the increase of the exergy efficiency of the system, as

494   shown in Fig. 4.

495   The influences of the BC turbine inlet pressure on the levelized exergy cost and the

496   system capital cost of the system are presented in Fig. 5. The levelized exergy cost for

497   the BC turbine output c_{Bt} increases with the increase of the BC turbine inlet pressure.

498   With the increase of the BC turbine output, the cost of the turbine increases, causing

499   the increase of the capital-cost-related part of c_{Bt}. Meanwhile, the increase of the

500   compressor power consumption causes the increase of the levelized exergy cost for

501   the CO_2 at the turbine inlet, resulting in the increase of the fuel-cost-related part of c_{Bt}.

502   As a result, c_{Bt} increases.

503   The levelized exergy cost for the ORC turbine product c_{Ot} increases with the

504   increase of the BC turbine inlet pressure. The decrease of the mass flow rate in the

505   DORC causes that less exergy is produced by the vapor generator 2. As a result, the

506   levelized exergy cost for the vapor at the high-pressure side of ORC turbine inlet

507   increases, which determines the increase of the fuel-cost-related part of the levelized

508   exergy for the ORC turbine power output. Thus, the levelized exergy cost for the ORC

509   turbine increases.

510   The system capital cost of increases with the increase of the BC turbine inlet

511   pressure. The increase of the BC turbine power output and the compressor power

512   consumption results in the increase of the BC turbine cost and compressor cost. The

513   increase of the mass flow rate in the ERC causes the increase of capital cost for the

514   evaporator and vapor generator 3. All the cost increase mention above accounts for

515   the increase of the system capital cost.

516   The levelized exergy cost for the system product decreases with the increase of BC

517   turbine inlet pressure as shown in Fig. 5. According to Eq. (31), the increase of c_{Ot}, c_{Bt}

518   and compressor power consumption could cause the increase of the fuel-cost-related

519   part of the levelized exergy cost for the system product. However, because of the large

520   increase of the system net power output, the capital-cost-related part and the

521   fuel-cost-related part decrease actually. Thus, the levelized exergy cost for the system

522   product decreases.

523   4.2.2.   Variations of thermal parameters in DORC.

524   The influences of inlet temperature at the high-pressure side of ORC turbine on the

525   output and the exergy efficiency of the system are shown in Fig. 6. The net power

526   output of the CBC remains unchanged. The reason is that the change of thermal

527   parameters in dual-pressure ORC can't affect the thermodynamic performance of the

528   CBC.

529   The net power output of the DORC cycle decreases with the increase of inlet

530   temperature at the high-pressure side of ORC turbine. With the increase of the vapor

531   temperature at the high-pressure ORC inlet, the mass flow rate of the organic working

532   fluid in the high-pressure side of DORC decreases. The decrease of organic working

533   fluid mass flow rate causes the decrease of the power output of the ORC turbine,

534   which further causes the decrease of the net power output of the DORC.

535   The cooling capacity of the ejector refrigeration cycle increases with the rise of

536   inlet temperature at the high-pressure side of ORC turbine. The decrease of the

537   organic working fluid mass flow rate in the DORC results in the decrease of the heat

538   transfer rate in the preheater. More heat is released in vapor generator 3 from the

539   jacket water to the working fluid in the ejector refrigeration cycle, leading to the

540   increase of the working fluid mass flow rate. Consequently, the cooling capacity of

541   the ejector refrigeration cycle increases.

542   The net power output of the CCP system decreases with the increase of inlet

543   temperature at the high-pressure side of ORC turbine. The increase of the working

544   fluid mass flow rate in the ERC causes the increase of the power consumption of

545   pump 4. Power output of the CBC keeps unchanged and dual-pressure ORC power

546   output decreases. According to Eq. (4), the net power output of the CCP system

547   decreases. The decrease of the CCP system net power output causes the decrease of

548   the exergy efficiency of the system, as shown in Fig. 6.

549   The influences of inlet temperature at the high-pressure side of ORC turbine on the

550   levelized exergy cost and the system capital cost of the system are presented in Fig. 7.

551   The levelized exergy cost for the ORC turbine (c_{Ot}) increases with the increase of inlet

552   temperature at the high-pressure side of ORC turbine. The can be explained by the

553   decrease of the decrease of the ORC turbine power output.

554   The levelized exergy cost for the BC turbine power output (c_{Bt}) increases with the

555   increase of inlet temperature at the high-pressure side of ORC turbine. Since the

556   decrease of the mass flow rate in the high-pressure side of ORC, the exergy of the

557   organic working fluid vapor generated by the vapor generator 2 decreases, causing the

558   increase of the levelized exergy cost of the vapor. The organic working fluid vapor is

559   heat by the BC turbine exhaust CO_2. Thus, the increase of the vapor levelized exergy

560   cost causes the increase of the levelized exergy cost for the exhaust CO_2. According to

561   Eq. (32), the increase of the levelized exergy cost for the exhaust CO_2 causes the

562   increase of the fuel-cost-related part of BC turbine levelized exergy cost. As a result,

563   the levelized exergy cost for the BC turbine power output increases.

564   The system capital cost decreases with the increase of inlet temperature at the

565   high-pressure side of ORC turbine. Because of the decrease of the organic working

566   fluid mass flow rate in the dual-pressure ORC, the cost of the ORC turbine and vapor

567   generator 2 decreases. Thus, the system capital cost decreases.

568   The levelized exergy cost for the system product ($c_{product}$) increases with the increase

569   of inlet temperature at the high-pressure side of ORC turbine, as shown in Fig. 7.

570   Since the increase of the levelized exergy cost for the BC turbine and ORC turbine

571   power output, the fuel-cost-related part of $c_{product}$ increases. Meanwhile, the large

572   decrease of the net power of the CCP system causes the increase of the

573   capital-cost-related part of $c_{product}$, according to Eq. (30). Thus, levelized exergy cost

574   for the system product increases.

575   The influences of inlet pressure at the high-pressure side of ORC turbine on the

576   output and the exergy efficiency of the system are presented in Fig. 8. The net power

577   output of the CBC keeps unchanged because of the unchanged thermal parameters in

578   the cycle.

579   The net power output of the DORC increase with the increase of inlet pressure at

580   the high-pressure side of ORC turbine. The increase of the evaporation pressure cuts

581   down the latent heat of the organic working fluid, which causes the increase of the

582   mass flow rate in the high-pressure side of the DORC. As a result, the net power

583   output of the ORC turbine increases, leading to the increase of the net power output of

584   the DORC.

585   Considering the increase of the DORC net power output and the unchanged CBC

586   net power output, the net power output of the whole system increases. Also, the

587   exergy efficiency of the system increases.

588   The increase of the mass flow rate in the DORC absorbs more heat from the jacket

589   water in the preheater. Thus, less heat is released in the vapor generator 3, causing the

590   decrease of the mass flow rate of the working fluid in the ERC. As a result, the

591   cooling capacity of the system decreases.

592   The influences of inlet pressure at the high-pressure side of ORC turbine on the

593   levelized exergy cost and system capital cost of the system are presented in Fig. 9.

594   The large increase of the net power output accounts for the decrease of the levelized

595   exergy cost for the ORC turbine power output. The increase of the mass flow rate of

596   the organic working fluid in the high-pressure side of the DORC means that more

597   exergy in the vapor is generated by the vapor generator 2. The levelized exergy cost

598   for the vapor at the vapor generator 2 outlet decreases. The exhaust CO_2 of the BC

599   turbine provides heat for the vapor. The decrease of the vapor levelized exergy cost

600   causes the decrease of the exhaust CO_2 levelized exergy cost. Meanwhile, the

601   decrease of the levelized exergy cost for the CO_2 causes results in the decrease of the

602   fuel-cost-related part of the levelized exergy cost for the BC turbine output. As a

603   result, the levelized exergy cost for the BC turbine power output decreases.

604   The increase of the ORC turbine power output and the increase of mass flow rate in

605   the DORC cause the increase of the turbine cost and the vapor generator 2 cost,

606   respectively. Thus, the system capital cost increases.

607   The levelized exergy cost for the system product decreases with the increase of

608   inlet pressure at the high-pressure side of ORC turbine. The decrease of the levelized

609   exergy cost for the ORC turbine power output and the BC turbine power output

610   accounts the decrease of the fuel-cost-related part of the levelized exergy cost for the

611   system product. The increase of the system net power outweighs the increase of the

612   system capital cost. Thus, the capital-cost-related part of the levelized exergy cost of

613   the system product. As a result, the levelized exergy cost of the system product

614   decreases.

615   The influences of inlet temperature at the low-pressure side of ORC turbine on the

616   output and the exergy efficiency of the system are presented in Fig. 10. Parameters

617   changes in the DORC can't affect the thermodynamic performance of the CBC. Thus,

618   the net power output of the CBC remains unchanged.

619   The net power of the DORC decreases with the increase of inlet temperature at the

620   low-pressure side of ORC turbine. The increase of the inlet temperature causes the

621   decrease of the mass flow rate in the low-pressure side of DORC, leading to the

622   decrease of the DORC net power output.

623   Considering the decrease of the DORC net power output and the unchanged CBC

624   net power output, the net power output of the whole system decreases. Also, the

625   exergy efficiency of the system decreases.

626   The cooling capacity of the ejector refrigeration cycle increases with the increase of

627   inlet temperature at the low-pressure side of ORC turbine. The increase of the inlet

628   temperature causes the decrease of the mass flow rate of the organic working fluid in

629   the low-pressure cycle. Thus, less heat is absorbed from the jacket water in the

630   preheater and more heat is released in vapor generator 3. The mass flow rate of the

631   working fluid in the ERC increases, leading to the increase of the cooling capacity.

632   The influences of inlet temperature at the low-pressure side of ORC turbine on the

633   levelized exergy cost and system capital cost of the system are presented in Fig. 11.

634   The levelized exergy cost for the BC turbine power output increases with the increase

635   of inlet temperature at the low-pressure side of ORC turbine. Though the enthalpy of

636   the organic working fluid increases with the increase of the low-pressure side inlet

637   temperature, the decrease of the mass flow rate causes the decrease of the exergy

638   provided by the vapor generator 1. Thus, the levelized exergy cost of the vapor

639   generated by vapor generator 1 increases. The levelized exergy cost for vapor in vapor

640   generator 2 is the equal to the levelized exergy cost for vapor in vapor generator 1. As

641   a result, the levelized exergy cost for the vapor generator 2 vapor increases, causing

642   the increase of the levelized exergy cost of the exhaust CO_2 after the BC turbine. The

643   increase of the levelized exergy cost for the exhaust CO_2 causes the increase of the

644   levelized exergy cost of the BC turbine power output.

645   The levelized exergy cost for the ORC turbine (c_{Ot}) increases with the increase of

646   inlet temperature at the low-pressure side of ORC turbine. As mentioned above, the

647   levelized exergy cost for the vapor at the low-pressure side of ORC turbine inlet

648   increases. Thus, the fuel-cost-related part of the levelized exergy cost for the ORC

649   turbine output increases. Also, the decrease of the ORC turbine power output causes

650   the increase both the fuel-cost-related part and the capital-cost-related part. As a result,

651   the levelized exergy cost for the ORC turbine power output increases.

652   The decrease of the mass flow rate and the ORC turbine power output cause the

653   decrease of the vapor generator 1 cost and the turbine cost. Thus, the capital cost of

654   the system decreases.

655   The levelized exergy cost for the system product increases with the increase of inlet

656   temperature at the low-pressure side of ORC turbine. The increase of c_{Bt} and c_{Ot} cause

657   the increase of the fuel-cost-related part of the levelized exergy cost for the system

658   product. Though, the decrease of the system capital cost causes the decrease of the

659   capital-cost-related part, its effect is less important. Thus, the increase of the

660   fuel-cost-related part determines the increase of the levelized exergy cost for the

661   system product.

662   The influences of the inlet pressure at the low-pressure side of ORC turbine on the

663   output and the exergy efficiency of the system are shown in Fig. 12. The net power of

664   the CBC keeps unchanged with the increase of the increase of the low evaporation

665   pressure. That reason is that the thermodynamic performance of the CBC is irrelevant

666   to the thermal parameters in DORC.

667   The net power output of the DORC increases with the increase of inlet pressure at

668   the low-pressure side of ORC turbine. The increase of inlet pressure at the

669   low-pressure side of ORC turbine causes the increase of the enthalpy drop of the

670   organic working fluid in the ORC turbine. Though the mass flow rate of the working

671   fluid decreases as well, the effect of the enthalpy drop is more important. Thus, the net

672   power of the DORC increases.

673   The unchanged CBC power output and the increase of the DORC power accounts

674   for the increase of the system net power output. The exergy efficiency of the system

675   increases as a result.

676   The cooling capacity increases with the increase of inlet pressure at the

677   low-pressure side of ORC turbine. Because of the decrease of the mass flow rate in

678   the DORC, less heat is absorbed in the preheater and more heat is provided in vapor

679   generator 3. Thus, the mass flow rate of the working fluid in the ERC increases,

680   causing the increase of the cooling capacity.

681   The influences of inlet pressure at the low-pressure side of ORC turbine on the

682   levelized exergy cost and system capital cost of the system are shown in Fig. 13. The

683   levelized exergy cost for the ORC turbine power output decreases with the increase of

684   inlet pressure at the low-pressure side of ORC turbine. The reason is that the decrease

685   of the mass flow rate in the DORC cuts down the capital cost of the vapor generator 1.

686   The power output of the DORC increases as well. Thus, both the capital-cost-related

687   part and the fuel-cost-related part of the system decrease. Consequently, the levelized

688   exergy cost of the ORC turbine power output decreases.

689   The levelized exergy cost for the BC turbine power output decreases with the

690   increase of the inlet pressure at the low-pressure side of ORC turbine. The decrease of

691   the levelized exergy cost causes the decrease of the levelized exergy cost for the vapor

692   at vapor generator 2 inlet. The vapor is heated by the exhaust CO_2 in the CBC. Thus,

693   the decrease of the vapor levelized exergy cost results in the decrease of the CO_2

694   levelized exergy cost which determines the fuel-cost-related part of the BC turbine

695   power levelized exergy cost. As a result, the levelized exergy cost for the BC turbine

696   power output decreases.

697   The increase of the ORC turbine power output causes the increase of the ORC

698   turbine cost. Meanwhile, the increase of the cooling capacity causes the increase of

699   the heat transfer area in the evaporator which requires the rise of the evaporator cost.

700   Thus, the capital cost of the system increases.

701   The levelized exergy cost for the system product decreases with the increase of

702   inlet pressure at the low-pressure side of ORC turbine. The decrease of the levelized

703   exergy cost of the BC turbine power output and ORC turbine power output cause the

704   decrease of the fuel-cost-related part of the system levelized exergy cost, which

705   determines the decrease of the levelized exergy cost for the system product.

706   4.2.3.   Variations of thermal parameters in ERC.

707   The influences of the ejector primary inlet pressure on the output and the exergy

708   efficiency of the system are shown in Fig. 14. Thermal parameters changes in the

709   ERC can' affect the thermodynamic performance of the CBC and DORC. Thus, the

710   net power output of the two cycles remain unchanged. With the increase of the ejector

711   primary inlet pressure, the power consumption of pump 4 increases, leading to the

712   slight decrease of the net power output of the whole system.

713   Since the entrainment ratio of the ejector increases with the increase of the ejector

714   primary inlet pressure. More working fluid in the is entrained to the ejector from the

715   ejector secondary inlet. Thus, the mass flow rate of the working fluid in the

716   evaporator increases, leading to the increase of the cooling capacity.

717   With the increase of the ejector primary inlet pressure, the power consumption of

718   pump 4 increase gradually. At first, the exergy loss in the pump 4 power consumption

719   is smaller than the exergy produced in the cooling capacity. Then, the power

720   consumption becomes larger. Thus, the exergy efficiency for the system increases at

721   first and then decreases with the increase of the ejector primary inlet pressure.

722   The influences of the ejector primary inlet pressure on the levelized exergy cost and

723   the system capital cost of the system are presented in Fig. 15. The increase of the

724   ejector primary inlet pressure can't affect the power output of the BC turbine and

725   ORC turbine. Thus, the levelized exergy cost for the BC turbine and ORC turbine

726   output remain unchanged.

727   The increase of the pump power consumption results in the increase of the pump 4

728   cost. The increase of the mass flow rate in the evaporator causes the increase of

729   evaporator cost. Thus, the system capital cost increases. The increase of the system

730   capital cost causes the increase of the capital-cost-related part of $c_{product}$. As a result,

731   the levelized exergy cost for the system product increases.

732   4.3.   System optimization

733   The parametric analysis reveals the potential of optimization for the CCP system.

734   With the increase of the BC turbine inlet temperature, the net power output of the

735   system increases while the cooling capacity decreases. With the increase of the inlet

736   temperature at the high-pressure side of ORC turbine, the net power output of the

737   system decreases while the cooling capacity increases. In this study, seven key

738   parameters (BC turbine inlet temperature, BC turbine inlet pressure, inlet temperature

739   at the high-pressure side of ORC turbine, inlet pressure at the high-pressure side of

740 ORC turbine, inlet temperature at the low-pressure side of ORC turbine, inlet pressure

741 at the low-pressure side of ORC turbine and the ejector primary inlet pressure) are

742 chosen as the variables to optimize the system. The ranges of these parameters are

743 listed in Table 6.

744   Considering that the levelized exergy cost reflects the thermodynamic and the

745 exergoeconomic aspect of the system, the levelized exergy cost for the system product

746 is selected as the objective function and genetic algorithm is selected to conduct the

747 single-objective optimization.

748   Genetic algorithm (GA) is an optimization method based on the natural biological

749 evaluation. [42] It simulates the natural genetic rules and searches the optimization

750 result in all the generation. The control parameters of the GA are listed in Table 7.

751   The optimization results of GA are listed in Table 8. It can be obtained that the

752 minimum levelized exergy cost for the system product $c_{product}$ is 53.25 \$ $(MWh)^{-1}$. The

753 exergy efficiency of the CCP system is 37.31% which is also desirable.

754 **5. Conclusion**

755   In this paper, a combined cooling and power system is developed. Seven

756 parameters (temperature and pressure at the inlet of BC turbine, temperature at the

757 high-pressure inlet and the low-pressure inlet of the ORC turbine, high-pressure side

758 and low-pressure side evaporation pressure in DORC and the ejector primary inlet

759 pressure) are selected to analyze the thermodynamic and exergoeconomic

760 performance of the system. Single-objective optimization is carried out with the help

761 of GA. The conclusions of this study are presented as follows:

762 (1) Both the increase of the BC turbine inlet temperature and pressure contribute to

763 the increase of the exergy efficiency and the decrease of the levelized exergy cost

764 for the system product.

765 (2) For both the high-pressure side and the low-pressure side of the DORC, the

766 increase of the ORC turbine inlet temperature causes the decrease of exergy

767 efficiency and the increase of the levelized exergy cost for the system product

768 while the increase of the ORC turbine inlet pressure results in the increase of

769 exergy efficiency and the decrease of the levelized exergy cost.

770 (3) The ERC performance analysis shows that the increase of the ejector primary

771 inlet pressure causes the increase of the cooling capacity and the decrease of

772 system net power output. Levelized exergy cost for the system product increases

773 with the increase of ejector primary inlet pressure.

774 (4) Single-objective optimization results show that the minimum levelized exergy

775 cost for the system product is obtained as 53.25 (MWh)^{-1}$ with net power output

776 of 374.37 kW, cooling capacity of 188.63 kW and system exergy efficiency of

777 37.31%.

781 **Appendix A**

782 This section shows the calculation of the heat transfer area in the heat exchangers

783 used in this study.

784 All the heat exchangers used in this study are tube-and-shell heat exchanger. The

785 thermodynamic properties of the working fluid vary with the heat transfer process.

786 Thus, to calculate the heat transfer area actually, the heat transfer processes are

787 discretized into a lot of small sections. In each section, the heat transfer area is small

788 and the thermodynamic properties are assumed to be constant.

789 For each section the heat transfer area is calculated as:

790
$$A_i = {Q_i} \Big/ {\left(\Delta T_i \cdot U_i \right)}$$
(B1)

791 where ΔT_i is the log-mean temperature difference (LMTD) and U_i is the overall heat

792 transfer coefficient.

793
$$\frac{1}{U_i} = \frac{1}{\alpha_{t,i}} + \frac{\delta}{\lambda} + \frac{1}{\alpha_{s,i}}$$
(B2)

794 In Eq. (B2) δ and λ represent the thickness of the tube and the thermal conductivity

795 of the tube wall, respectively. $\alpha_{t,i}$ is the convection heat transfer coefficient in the tube

796 side and $\alpha_{s,i}$ is the convection heat transfer coefficient in the shell side.

797 For different heat transfer process, the convection heat transfer coefficient has

798 different format. We classify the heat transfer processes into single-phase heat transfer

799 process and two-phase heat transfer process. In gas heater, precooler and the preheater,

800 single-phase heat transfer process happens. In evaporator, two-phase heat transfer

801 process occurs. In vapor generators and the condensers, both the single-phase and the

802 two-phase heat transfer process happen.

803 In the single-phase heat transfer process, the convection heat transfer coefficient in

804 the tube side and the shell side are expressed as [43]:

805 $\alpha_{t,i} = \dfrac{\lambda \cdot Nu}{D_i}$ (B3)

806 $\alpha_{s,i} = 0.36 \left(\dfrac{\lambda}{D_{es}} \right) \cdot \left(\dfrac{D_{es} \cdot G_s}{\mu} \right)^{0.55} \cdot Pr^{\frac{1}{3}} \cdot \left(\dfrac{\mu}{\mu_w} \right)^{0.14}$ (B4)

807 In Eq. (B3), the Nusselt number is calculated as [44,45]:

808 $Nu = \left[\dfrac{(f/8) \cdot Re \cdot Pr}{12.7(f/8)^{0.5} \cdot (Pr^{2/3} - 1) + 1.07} \right], \quad for\ Re < 10^4$ (B5)

809 $Nu = \left[\dfrac{(f/8) \cdot (Re - 1000) \cdot Pr}{12.7(f/8)^{0.5} \cdot (Pr^{2/3} - 1) + 1.07} \right], \quad for\ 10^4 < Re < 5 \times 10^6$ (B6)

810 where f is the Darcy frication factor, Re is the Reynolds and Pr is the Prandtl number.

811 In Eq. (B4), D_{es} is the equivalent diameter of the shell, being expressed as:

812 $D_{es} = \dfrac{1.10 Pt^2}{D_{out,i}} - D_{out,i}$ (B7)

813 where Pt is the center distance between the tubes.

814 Evaporation and condensation are two different two-phase heat transfer processes.

815 In this study, the cold organic working fluid flows in the tubes of the heat exchangers.

816 The convection heat transfer coefficient of evaporation and condensation are

817 expressed as [46,47]:

818 $\alpha_{ev,i} = 0.023 \left[\dfrac{G(1-x)}{\mu_l} \right]^{0.8} \cdot Pr_l^{0.4} \cdot \dfrac{\lambda_l}{d} \cdot \left[1 + 3000 Bo^{0.86} + 1.12 \left(\dfrac{x}{1-x} \right)^{0.75} \cdot \left(\dfrac{\rho_l}{\rho_v} \right)^{0.41} \right]$ (B8)

819 $\alpha_{cond,i} = 0.023 \left[\dfrac{G(1-x)}{\mu_l} \right]^{0.8} \cdot Pr_l^{0.4} \cdot \dfrac{\lambda_l}{d} \cdot \left[(1-x)^{0.8} + \dfrac{3.8 x^{0.76} (1-x)0.04}{P_r^{0.38}} \right]$ (B9)

820   In Eq. (B9), P_r is the reduced pressure. In Eq. (B8) Bo is the boiling number, being

821   expressed as:

822    $$Bo = \frac{q_{\mathrm{m}}}{G \cdot r_{\mathrm{f}}}$$ (B10)

823   **Appendix B**

824   The constants for component capital cost calculation are list in Table B1.

825   **Reference**

826   [1] Heywood J. B. Internal combustion engine fundamentals. New York:

827   McGraw-Hill; 1988.

828   [2] Chao H, Chao L, Hong G, Hui X, You L, Shuang W. The optimal evaporation

829   temperature and working fluids for subcritical Organic Rankine Cycle. Energy 2012;

830   38: 136-143.

831   [3] Bombarda P, Invernizzi C, Pietra C. Heat recovery from Diesel engines: A

832   thermodynamic comparison between Kalina and ORC cycles. Applied Thermal

833   Engineering 2010; 30: 212-219.

834   [4] Kalyan K, Pedro J, Sundar R. Analysis of exhaust waste heat recovery from a dual

835   fuel low temperature combustion engine using an Organic Rankine Cycle. Energy

836   2010; 35: 2387-2399.

837   [5] Wei M, Fang J, Ma C, Danish S. Waste heat recovery from heavy-duty diesel

838   engine exhaust gases by medium temperature ORC system. Science China

839   Technological Sciences 2011; 54: 2746-2753.

840   [6] Srinivasan K, Mago P, Zdaniuk G, Chamra L, Midkiff K. Improving the Efficiency

841   of the Advanced Injection Low Pilot Ignited Natural Gas Engine Using Organic

842   Rankine Cycles. 2008; 130: 022201.

843   [7] Tian H, Shu G, Wei H, Liang X, Liu L. Fluids and parameters optimization for the

844   organic Rankine cycles (ORCs) used in exhaust heat recovery of Internal Combustion

845   Engine (ICE). Energy 2012; 47: 125-136.

846   [8] Vaja I, Gambarotta A. Internal Combustion Engine (ICE) bottoming with Organic

847   Rankine Cycles (ORCs). Energy 2010; 35(2): 1084-1093.

848   [9] Rosset K, Mounier V, Guenat E, Schiffmann J. Multi-objective optimization of

849   turbo-ORC systems for waste heat recovery on passenger car engines. Energy 2018;

850   159: 751-765.

851   [10] Zhang H G, Wang E H, Fan B Y. A performance analysis of a novel system of a

852   dual loop bottoming organic Rankine cycle (ORC) with a light-duty diesel engine.

853   Applied Energy 2013;102: 1504-1513.

854   [11] Yang F, Cho H, Zhang H, Zhang J. Thermoeconomic multi-objective

855   optimization of a dual loop organic Rankine cycle (ORC) for CNG engine waste heat

856   recovery. Applied Energy 2017; 205: 1100-1118.

857   [12] Ge Z, Li J, Liu Q, Duan Y, Yang Z. Thermodynamic analysis of dual-loop

858   organic Rankine cycle using zeotropic mixtures for internal combustion engine waste

859   heat recovery. Energy Conversion and Management 2018; 166: 201-214.

860 [13] Chen T, Zhuge W, Zhang Y, Zhang L. A novel cascade organic Rankine cycle

861 (ORC) system for waste heat recovery of truck diesel engines. Energy Conversion and

862 Management 2017;138: 210-223.

863 [14] Mansoury M, Jafarmadar S, Khalilarya S. Energetic and exergetic assessment of

864 a two-stage Organic Rankine Cycle with reactivity-controlled compression ignition

865 engine as a low temperature heat source. Energy Conversion and Management 2018;

866 166: 201-214.

867 [15] Seyedkavoosi S, Javan S, Kota K. Exergy-based optimization of an organic

868 Rankine cycle (ORC) for waste heat recovery from an internal combustion engine

869 (ICE). Applied Thermal Engineering 2017; 126: 447-457.

870 [16] Rajabloo T, Davide B, Paolo lora. Effect of a partial thermal decomposition of

871 the working fluid on the performances of ORC power plants. Energy 2017;

872 133:1013-1026.

873 [17] Shu G, Zhao M, Tian H, Wei H, Liang X, Huo Y, et al. Experimental

874 investigation on thermal OS/ORC (Oil Storage/Organic Rankine Cycle) system for

875 waste heat recovery from diesel engine. Energy 2016; 107: 693-706.

876 [18] Wang X, Tian H, Shu G. Part-load performance prediction and operation strategy

877 design of organic Rankine cycles with a medium cycle used for recovering waste heat

878 from gaseous fuel engines. Energies 2016; 9: 527.

879 [19] Miller E, Hendricks T, Peterson R. Modeling Energy Recovery Using

880 Thermo-electric Conversion Integrated with an Organic Rankine Bottoming Cycle.

881 Journal of Electron Mater 2009; 38: 1206-1213.

882 [20] Miller E, Hendricks T, Wang H, Peterson R. Integrated dual-cycle energy

883 recovery using thermoelectric conversion and an organic Rankine bottoming cycle.

884 Proceedings of the Institution of Mechanical Engineers, Part A: Journal of Power and

885 Energy 2011; 225: 33-43.

886 [21] Shu G, Wang X, Tian H. Theoretical analysis and comparison of Rankine cycle

887 and different organic Rankine cycles as waste heat recovery system for a large

888 gaseous fuel internal combustion engine. Applied Thermal Engineering 2016; 108:

889 525-537.

890 [22] Galindo J, Guardiola C, Dolz V, Kleut P. Further analysis of a

891 compression-expansion machine for a Brayton Waste Heat Recovery cycle on an IC

892 engine. Applied Thermal Engineering 2018; 128: 345-356.

893 [23] Yu G, Shu G, Tian Hua, Wei H, Liu L. Simulation and thermodynamic analysis

894 of a bottoming Organic Rankine Cycle (ORC) of diesel engine (DE). Energy 2013; 51:

895 281-290.

896 [24] Ma J, Liu L, Zhu T, Zhang T. Cascade utilization of exhaust gas and jacket water

897 waste heat from an Internal Combustion Engine by a single loop Organic Rankine

898 Cycle system. Applied Thermal Engineering 2016; 107: 218-226.

899 [25] Chen Y, Han W, Jin H. Investigation of an ammonia-water combined power and

900 cooling system driven by the jacket water and exhaust gas heat of an internal

901 combustion engine. International Journal of Refrigeration 2017; 82: 174-188.

902   [26] Salek F, Moghaddam A, Naserian M. Thermodynamic analysis of diesel engine

903   coupled with ORC and absorption refrigeration cycle. Energy Conversion and

904   Management 2017; 140: 240-246.

905   [27] Wang J, Dai Y, Sun Z, A theoretical study on a novel combined power and ejector

906   refrigeration cycle. International Journal of Refrigeration 2009; 32: 1186-1194.

907   [28] Ahmadi P, Dincer I, Rosen M. Performance assessment and optimization of a

908   novel integrated multigeneration system for residential buildings. Energy and

909   Buildings 2013; 67: 568-578.

910   [29] Dai Y, Wang J, Gao L. Parametric optimization and comparative study of organic

911   Rankine cycle (ORC) for low grade waste heat recovery. Energy Conversion

912   Management 2009; 50: 576-582.

913   [30] Shu G, Zhao M, Tian H, Huo Y, Zhu W. Experimental comparison of R123 and

914   R245fa as working fluids for waste heat recovery from heavy-duty diesel engine.

915   Energy 2016; 115: 756-769.

916   [31] Zhang J, Zhang H, Yang K, Yang F, Wang Z, Zhao G, et al. Performance analysis

917   of regenerative organic Rankine cycle (RORC) using the pure working fluid and the

918   zeotropic mixture over the whole operating range of a diesel engine. Energy

919   Conversion Management 2014; 84: 282-294.

920   [32] Adrian Bejan GT, Moran Michael. Thermal design and optimization. New York:

921   Jogn Wiley & Sons; 1996.

922   [33] Turton R. Analysis, synthesis, and design of chemical processes. 3rd ed. Upper

923   Saddle River, N.J: Prentice Hall; 2009.

924 [34] Li J, Ge Z, Liu Q, Duan Y, Yang Z. Thermo-economic performance analyses and

925 comparison of two turbine layouts for organic Rankine cycles with dual-pressure

926 evaporation. Energy Conversion and Management, 2018; 164: 603-614.

927 [35] http://www.chemengonline.com/pci-home

928 [36] Sheng Z, Huai W, Tao G. Performance comparison and parametric optimization

929 of subcritical organic Rankine cycle (ORC) and transcritical power cycle system for

930 low-temperature geothermal power generation. Applied Energy

931 2011;88(8):2740-2754.

932 [37] Tempesti D, Fiaschi D. Thermo-economic assessment of a micro CHP system

933 fueled by geothermal and solar energy. Energy 2013; 58: 45-51.

934 [38] Velez F, Segovia JJ, Martin MC, Antonlin G, Chejne F, Quijano A. A technical,

935 economical and market review of organic Rankine cycles for the conversion of

936 low-grade heat for power generation. Renewable and Sustainable Energy Reviews,

937 2012; 16:4175-4189.

938 [39] Akbari D, Mahmoudi M. Thermoeconomic analysis & optimization of the

939 combined supercritical CO2 (carbon dioxide) recompression Brayton/ organic

940 Rankine cycle. Energy 2014; 78:501-512.

941 [40] Zare V, Mahmoudi M, Yari M. An exergoeconomic investigation of waste heat

942 recovery from the Gas Turbine-Modular Helium Reactor (GT-MHR) employing an

943 ammonia–water power/cooling cycle. Energy 2013;61. 397-409.

944   [41] Lemmon EW, Huber ML, McLinden MO. NIST standard reference database 23,

945   reference fluid thermodynamic and transport properties (REFPROP). Version 9.1.

946   National Institute of Standards and Technology; 2010

947   [42] Wang J, Dai Y, Gao L. Parametric analysis and optimization for a combined

948   power and refrigeration cycle. Applied Energy 2008;85(11):1071-1085

949   [43] Kern DQ. Process heat transfer. New York: McGraw-Hill; 1950

950   [44] Kandylas IP, Stamatelos AM. Engine exhaust system design based on heat

951   transfer computation. Energy Conversion Management 1999; 40:1057-1072.

952   [45] Incropera FP, DeWitt DP. Fundamentals of heat and mass transfer. New York:

953   Wiley; 2002

954   [46] Gungor KE, Winterton RHS. Simplified general correlation for saturated flow

955   boiling and comparisons of correlations with data. Chemical Engineering Research

956   and Design, 1987; 65:148-156.

957   [47] Shah MM. A general correlation for heat transfer during film condensation inside

958   pipes. International Journal of Heat and Mass Transfer 1979; 22:547-556.

959

990

Table 1 Energy and exergy models for each component in CCP system

Component	Energy equation	E_F	E_P	E_D	E_L
Gas heater	$M_{g1} \cdot (h_{g1} - h_{g2}) = M_2 \cdot (h_3 - h_2)$	$E_{g1} - E_{g2}$	$E_3 - E_2$	$E_{g1} + E_2 - E_3 - E_{g2}$	/
BC turbine	$W_{Bt} = M_3 \cdot (h_3 - h_4) = M_3 \cdot (h_3 - h_{4s}) \cdot \eta_{Bt}$	$E_3 - E_4$	W_{Bt}	$E_3 - E_4 - W_{Bt}$	/
Vapor generator 2	$M_4 \cdot (h_4 - h_5) = M_9 \cdot (h_{10} - h_9)$	$E_4 - E_5$	$E_{10} - E_9$	$E_4 + E_9 - E_5 - E_{10}$	/
Precooler	$M_1 \cdot (h_5 - h_1) = M_{26} \cdot (h_{27} - h_{26})$	/	/	$E_5 + E_{26} - E_1 - E_{27}$	$E_{27} - E_{26}$
Compressor	$W_{comp} = M_1 \cdot (h_2 - h_1) = M_1 \cdot (h_{2s} - h_1) / \eta_{comp}$	W_{comp}	$E_2 - E_1$	$E_1 - E_2 + W_{comp}$	/
Vapor generator 1	$M_{g2} \cdot (h_{g2} - h_{g3}) = M_8 \cdot (h_{11} - h_8)$	$E_{g2} - E_{g1}$	$E_{11} - E_8$	$E_{g2} + E_8 - E_{11} - E_{g3}$	/
ORC turbine	$W_{Ot} = M_{10} \cdot (h_{10} - h_{12}) + M_{11} \cdot (h_{11} - h_{12})$	$E_{10} + E_{11} - E_{12}$	W_{Ot}	$E_{10} + E_{11} - E_{12} + W_{Ot}$	/
Condenser 1	$M_{12} \cdot (h_{12} - h_{13}) = M_{28} \cdot (h_{29} - h_{28})$	/	/	$E_{12} + E_{28} - E_{13} - E_{29}$	$E_{29} - E_{28}$
Pump 1	$W_{p1} = M_{13} \cdot (h_{14} - h_{13}) = M_{13} \cdot (h_{14s} - h_{13}) / \eta_{p1}$	W_{p1}	$E_{14} - E_{13}$	$E_{13} - E_{14} + W_{p1}$	/
Preheater	$M_{15} \cdot (h_{15} - h_{14}) = M_{w1} \cdot (h_{w1} - h_{w2})$	$E_{w1} - E_{w2}$	$E_{15} - E_{14}$	$E_{w1} + E_{14} - E_{15} - E_{w2}$	/
Pump 2	$W_{p2} = M_7 \cdot (h_9 - h_7) = M_7 \cdot (h_{9s} - h_7) / \eta_{p2}$	W_{p2}	$E_9 - E_7$	$E_7 - E_9 + W_{p2}$	/
Pump 3	$W_{p3} = M_6 \cdot (h_8 - h_6) = M_6 \cdot (h_{8s} - h_6) / \eta_{p3}$	W_{p3}	$E_8 - E_6$	$E_6 - E_8 + W_{p3}$	/
Vapor generator 3	$M_{23} \cdot (h_{23} - h_{22}) = M_{w2} \cdot (h_{w2} - h_{w3})$	$E_{w2} - E_{w3}$	$E_{23} - E_{22}$	$E_{w2} + E_{22} - E_{23} - E_{w3}$	/
Condenser 2	$M_{16} \cdot (h_{16} - h_{17}) = M_{30} \cdot (h_{31} - h_{30})$	/	/	$E_{16} + E_{30} - E_{17} - E_{31}$	$E_{31} - E_{30}$
Valve	$h_{19} = h_{20}$	/	/	$E_{19} - E_{20}$	/
Pump 4	$W_{p4} = M_{22} \cdot (h_{22} - h_{18}) = M_{22} \cdot (h_{22s} - h_{18}) / \eta_{p4}$	W_{p4}	$E_{22} - E_{18}$	$E_{18} - E_{22} + W_{p4}$	/
Ejector	$M_{16} \cdot h_{16} = M_{23} \cdot h_{23} + M_{21} \cdot h_{21}$	$E_{23} + E_{21}$	E_{16}	$E_{23} + E_{21} - E_{16}$	/
Evaporator	$M_{20} \cdot (h_{21} - h_{20}) = M_{24} \cdot (h_{24} - h_{25})$	$E_{20} - E_{21}$	$E_{25} - E_{24}$	$E_{20} + E_{24} - E_{21} - E_{25}$	/

Table 2 Cost balance and auxiliary relation [32] for each component of CCP system

Component	Cost balance	Auxiliary relation

Gas heater	$c_{g2} \cdot E_{y,g2} + c_3 \cdot E_{y,3} = c_{g1} \cdot E_{y,g1} + c_2 \cdot E_{y,2} + Z_{gh}$	$c_{g1}=c_{g2}=0$
Vapor generator 2	$c_5 \cdot E_{y,5} + c_{10} \cdot E_{y,10} = c_4 \cdot E_{y,4} + c_9 \cdot E_{y,9} + Z_{vg,2}$	$c_4=c_5$
BC turbine	$c_4 \cdot E_{y,4} + c_{Bt} \cdot W_{y,Bt} = c_3 \cdot E_{y,3} + Z_{Bt}$	$c_4=c_3$
Precooler	$c_1 \cdot E_{y,1} + c_{26} \cdot E_{y,26} = c_5 \cdot E_{y,5} + c_{27} \cdot E_{y,27} + Z_{prec}$	$c_1=c_5$
Compressor	$c_2 \cdot E_{y,2} = c_1 \cdot E_{y,1} + c_{elec,1} \cdot W_{y,comp} + Z_{comp}$	$c_{elec,1}=c_{Bt}$
Vapor generator 1	$c_{g3} \cdot E_{y,g3} + c_{11} \cdot E_{y,11} = c_{g2} \cdot E_{y,g2} + c_8 \cdot E_{y,8} + Z_{vg,1}$	$c_{g2}=c_{g3}$
ORC turbine	$c_{12} \cdot E_{y,12} + c_{Ot} \cdot W_{y,Ot} = c_{11} \cdot E_{y,11} + c_{10} \cdot E_{y,10} + Z_{Ot}$	$c_{10}=c_{11}=c_{12}$
Pump 1	$c_{14} \cdot E_{y,14} = c_{13} \cdot E_{y,13} + c_{elec,3} \cdot W_{y,pump1} + Z_{pump1}$	$c_{elec,3}=c_{Ot}$
Condenser 1	$c_{13} \cdot E_{y,13} + c_{29} \cdot E_{y,29} = c_{28} \cdot E_{y,28} + c_{12} \cdot E_{y,12} + Z_{cond1}$	$c_{13}=c_{12}$
Preheater	$c_{w2} \cdot E_{y,w2} + c_{15} \cdot E_{y,15} = c_{w1} \cdot E_{y,w1} + c_{14} \cdot E_{y,14} + Z_{preh}$	$c_{w1}=c_{w2}=0$
Pump 2	$c_9 \cdot E_{y,9} = c_7 \cdot E_{y,7} + c_{elec,2} \cdot W_{y,pump2} + Z_{pump2}$	$c_{elec,2}=c_{Ot}$
Pump 3	$c_8 \cdot E_{y,8} = c_6 \cdot E_{y,6} + c_{elec,3} \cdot W_{y,pump3} + Z_{pump3}$	$c_{elec,3}=c_{Ot}$
Vapor generator 3	$c_{w3} \cdot E_{y,w3} + c_{23} \cdot E_{y,23} = c_{w2} \cdot E_{y,w2} + c_{22} \cdot E_{y,22} + Z_{vg,3}$	$c_{w3}=c_{w2}$
Valve	/	$c_{19}=c_{20}$
Pump 4	$c_{22} \cdot E_{y,22} = c_{18} \cdot E_{y,18} + c_{elec,3} \cdot W_{y,pump4} + Z_{pump4}$	$c_{elec,4}=c_{Ot}$
Condenser 2	$c_{17} \cdot E_{y,17} + c_{31} \cdot E_{y,31} = c_{30} \cdot E_{y,30} + c_{16} \cdot E_{y,16} + Z_{cond2}$	$c_{16}=c_{17}$
Ejector	$c_{16} \cdot E_{y,16} = c_{23} \cdot E_{y,23} + c_{21} \cdot E_{y,21}$	/
Evaporator	$c_{21} \cdot E_{y,21} + c_{25} \cdot E_{y,25} = c_{20} \cdot E_{y,20} + c_{24} \cdot E_{y,24} + Z_{ev}$	$c_{20}=c_{21}$

993   **Table 3** Condition of simulation for the CCP system

Term	Value
Ambient temperature (℃)	20
Ambient pressure (MPa)	0.101

Compressor inlet temperature (℃)	35
BC turbine inlet temperature (℃)	400
BC turbine inlet pressure (MPa)	18
BC turbine outlet pressure (MPa)	8
Inlet temperature at the high-pressure side of ORC turbine (℃)	150
Inlet pressure at the high-pressure side of ORC turbine (MPa)	1.6
Inlet temperature at the low-pressure side of ORC turbine (℃)	100
Inlet pressure at the low-pressure side of ORC turbine (MPa)	1.0
Outlet pressure of pump 1 (MPa)	0.9
Ejector primary inlet pressure (MPa)	0.4
Terminal temperature difference at gas heater outlet (℃)	100
Pinch point temperature difference in vapor generator 1 (℃)	30
Pinch point temperature difference in vapor generator 2 (℃)	30
Pinch point temperature difference in vapor generator 3 (℃)	25
Condensation temperature of condenser 1 (℃)	30
Condensation temperature of condenser 2 (℃)	30
Evaporation temperature of evaporator (℃)	5
Isentropic efficiency of BC turbine (%)	80
Isentropic efficiency of ORC turbine (%)	80
Isentropic efficiency of compressor (%)	80
Isentropic efficiency of pump 1 (%)	75
Isentropic efficiency of pump 2 (%)	75

| Isentropic efficiency of pump 3 (%) | 75 |
| Inlet temperature of cooling water (℃) | 20 |

Table 4 Main parameters of the engine [8]

Parameters	Value
Power output (kW)	2928
Rotation ($r(min)^{-1}$)	1000
Exhaust gas temperature (℃)	470
Exhaust gas mass flow rate ($kg\ s^{-1}$)	4.35
Temperature of jacket water (℃)	90/79
Mass flow rate of jacket water ($kg\ s^{-1}$)	25

Table 5 Composition of the exhaust gas [8]

Composition	Molecular ($g(mol)^{-1}$)	Fraction (%)
O_2	32.00	9.3
CO_2	44.00	9.1
H_2O	18.01	7.4
N_2	28.01	74.2

Table 6 Parameters for GA

Ranges of the decision variables	Range
BC turbine inlet temperature (℃)	330-440
BC turbine inlet pressure (MPa)	15-20
Inlet temperature at the high-pressure side of ORC turbine (℃)	130-180
Inlet pressure at the high-pressure side of ORC turbine (MPa)	1.4-2

Inlet temperature at the low-pressure side of ORC turbine (℃)	90-150
Inlet pressure at the low-pressure side of ORC turbine (MPa)	0.9-1.3
Ejector primary inlet pressure (MPa)	0.3-1

997 **Table 7** Control parameters of GA

Tuning parameters	Value
Population size	20
Mutation probability	0.01
Crossover probability	0.8
Stop generation	200

998 **Table 8** Single-objective optimization results

Term	Value
BC turbine inlet temperature (℃)	425.457
BC turbine inlet pressure (MPa)	20
Inlet temperature at the high-pressure side of ORC turbine (℃)	144.315
Inlet pressure at the high-pressure side of ORC turbine (MPa)	1.847
Inlet temperature at the low-pressure side of ORC turbine (℃)	100.032
Inlet pressure at the low-pressure side of ORC turbine (MPa)	1.264
Ejector primary inlet pressure (MPa)	0.537
Net power output (kW)	374.37
Cooling capacity (kW)	188.63
Exergy efficiency (%)	37.31
Levelized exergy cost ($ (MWh)$^{-1}$)	53.25

999 **Table B1** Constants for component costs [32]

Constant	Value	Constant	Value	Constant	Value
$B_{1,he}$	1.63	$K_{3,pump}$	0.1538	$C_{3,he}$	0.08183
$B_{2,he}$	1.66	$K_{1,turb}$	2.7051	$C_{1,pump}$	-0.3635
$B_{1,pump}$	1.89	$K_{2,turb}$	1.4398	$C_{2,pump}$	0.3957
$B_{2,pump}$	1.35	$K_{3,turb}$	-0.1776	$C_{3,pump}$	-0.0026
$K_{1,he}$	4.3247	$K_{1,comp}$	2.2897	$F_{M,he}$	1.0
$K_{2,he}$	-0.3030	$K_{2,comp}$	1.3604	$F_{BM,turb}$	3.5
$K_{3,he}$	0.1634	$K_{3,comp}$	-0.1027	$F_{BM,comp}$	2.7
$K_{1,pump}$	3.3892	$C_{1,he}$	0.03881	$F_{M,pump}$	2.2
$K_{2,pump}$	0.0536	$C_{2,he}$	-0.11272		

1000

1001

1002 **Fig. 1.** Schematic diagram of the CCP system

1003

1004 **Fig. 2.** Influences of BC turbine inlet temperature on the output and the exergy

1005 efficiency of the system.

1006
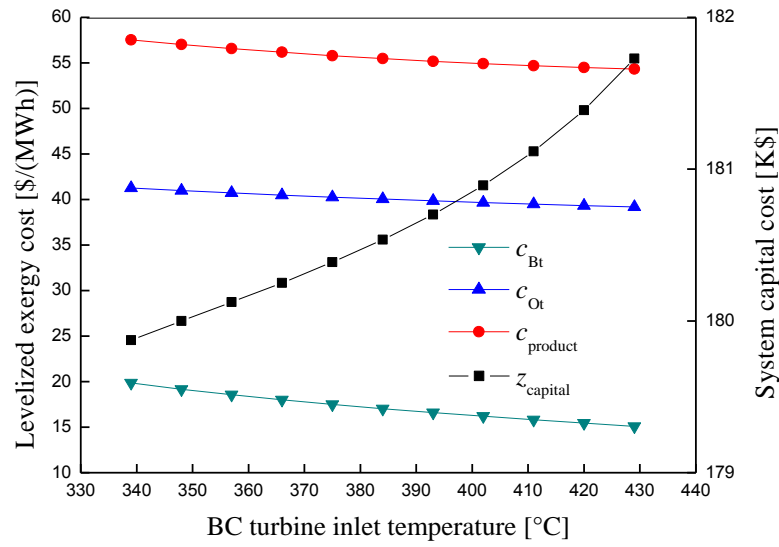
1007 **Fig. 3.** Influences of BC turbine inlet temperature on the levelized exergy cost and the

1008 system capital cost of the system.

1009
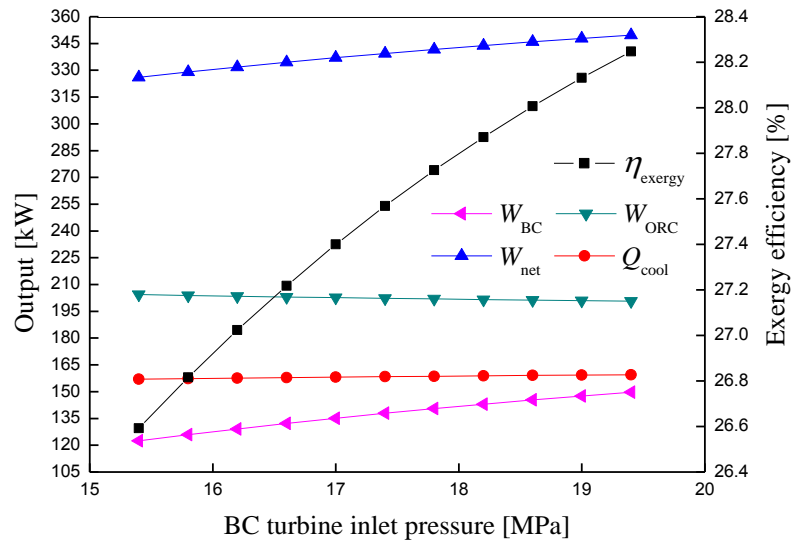
1010 **Fig. 4.** Influences of BC turbine inlet pressure on the output and the exergy efficiency
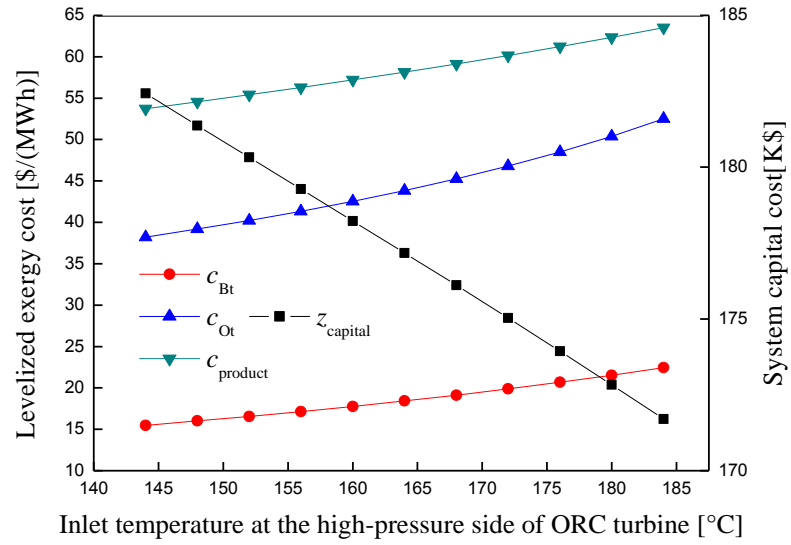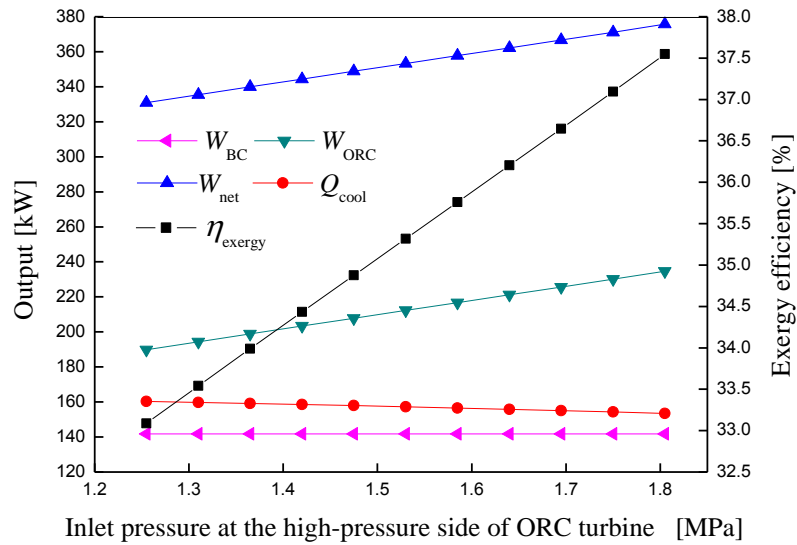
1011 of the system.

1012
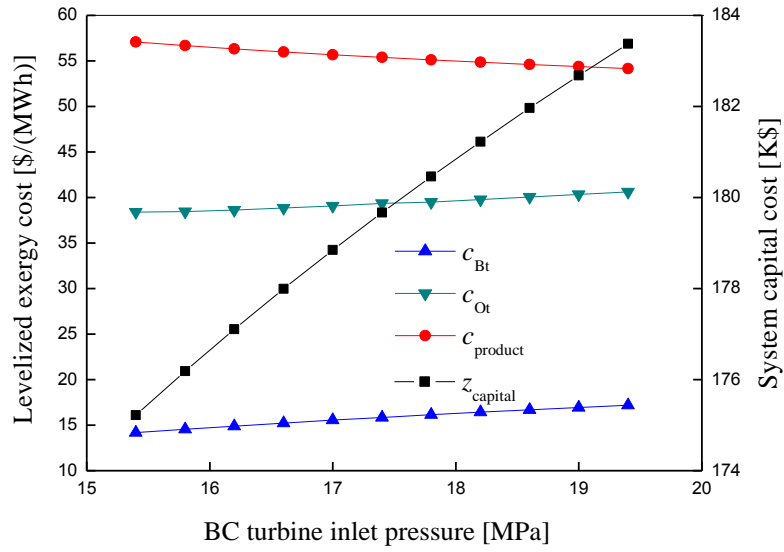
1013   **Fig. 5.** Influences of BC turbine inlet pressure on the levelized exergy cost and the

1014   system capital cost of the system.

1015
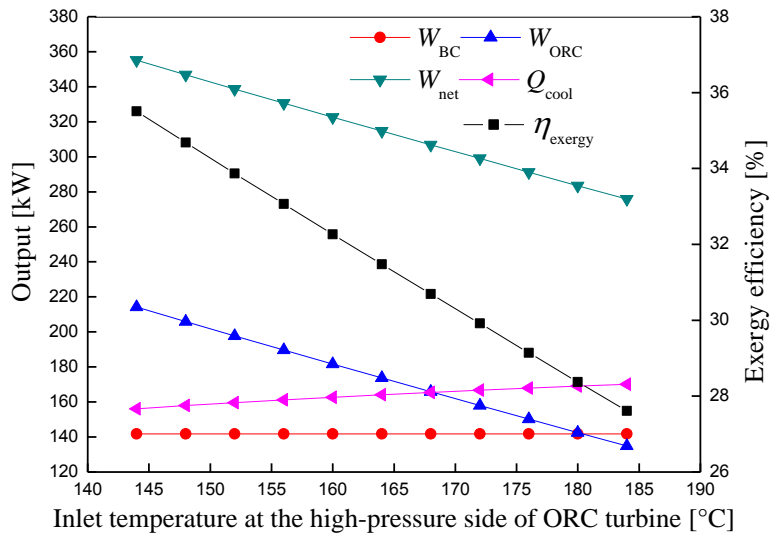
1016   **Fig. 6.** Influences of inlet temperature at the high-pressure side of ORC turbine on the

1017   output and the exergy efficiency of the system.

1018

1019   **Fig. 7.** Influences of inlet temperature at the high-pressure side of ORC turbine on the

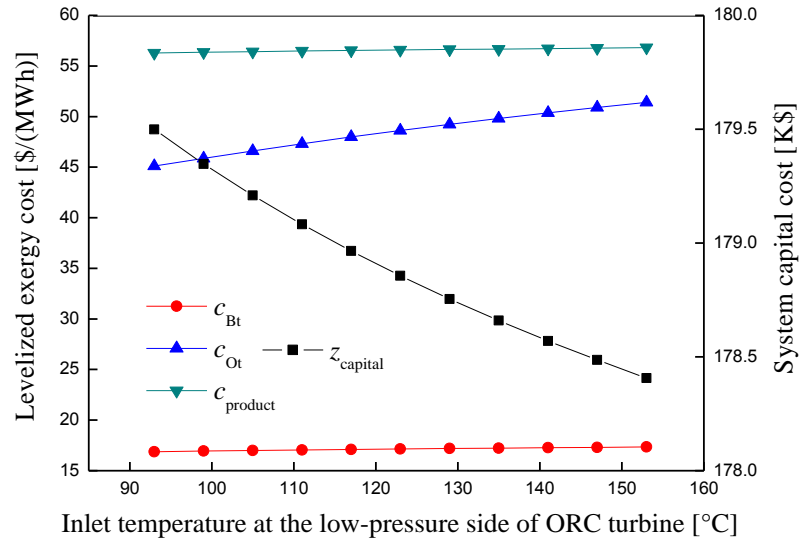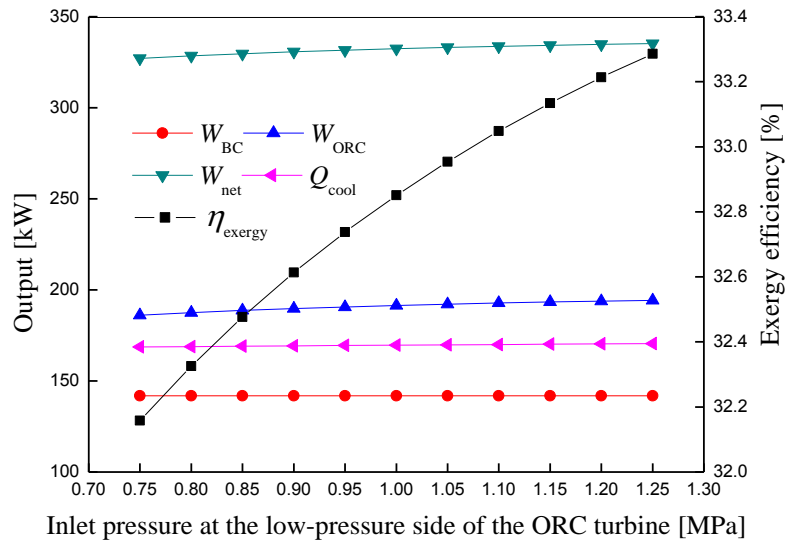1020   levelized exergy cost and the system capital cost of the system.

1021

1022   **Fig. 8.** Influences of inlet pressure at the high-pressure side of ORC turbine on the

1023   output and the exergy efficiency of the system.

1024
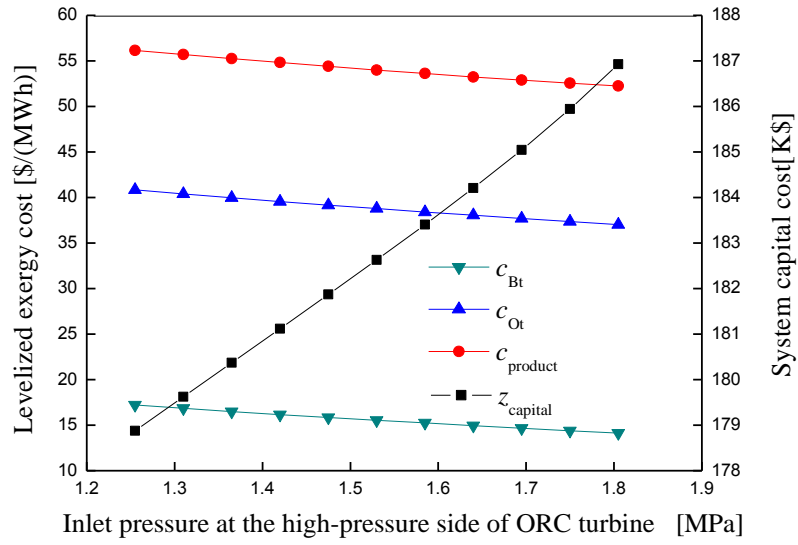
1025   **Fig. 9.** Influences of inlet pressure at the high-pressure side of ORC turbine on the

1026   levelized exergy cost and the system capital cost of the system.
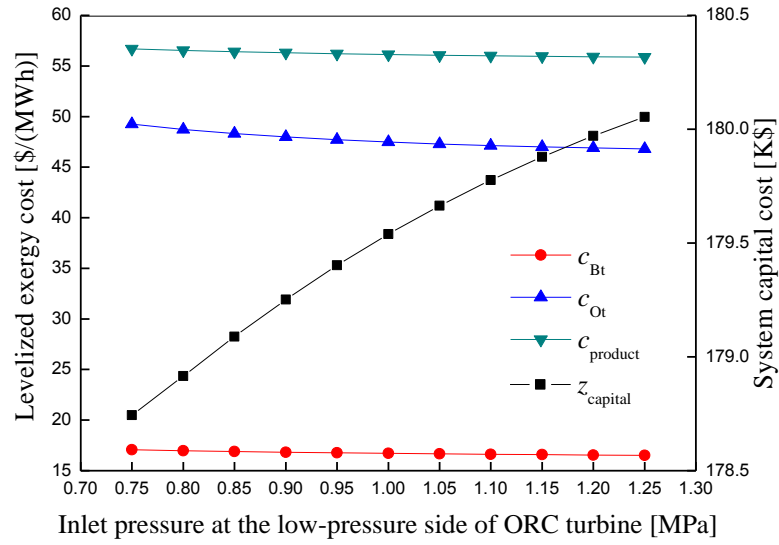

1027
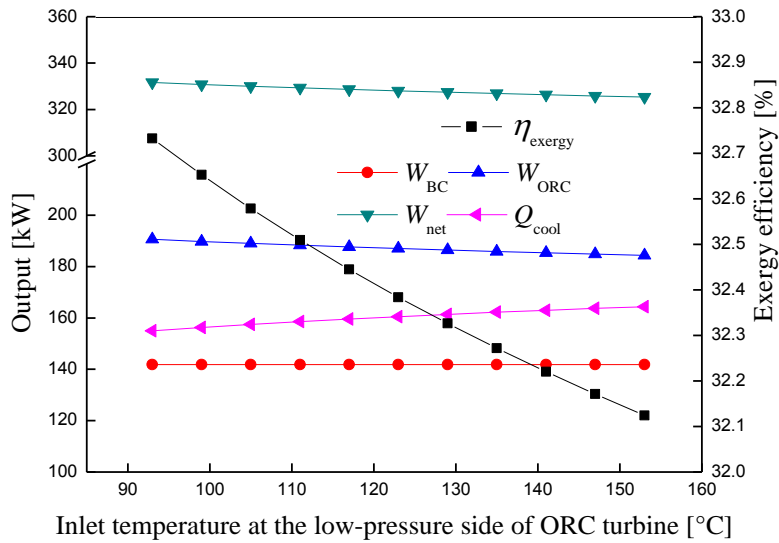
1028   **Fig. 10.** Influences of inlet temperature at the low-pressure side of ORC turbine on the

1029   output and the exergy efficiency of the system.

1030

1031 **Fig. 11.** Influences of inlet temperature at the low-pressure side of ORC turbine on

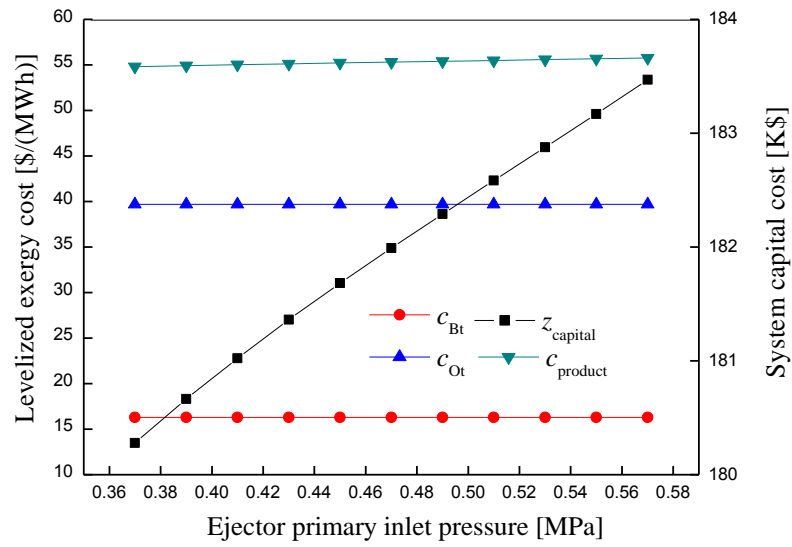1032 the levelized exergy cost and system capital cost of the system.

1033

1034 **Fig. 12.** Influences of inlet pressure at the low-pressure side of ORC turbine on the

1035 output and the exergy efficiency of the system.

1036

1037   **Fig. 13.**   Influences of the inlet pressure at the low-pressure side of ORC turbine on

1038   the levelized exergy cost and system capital cost of the system.

1039
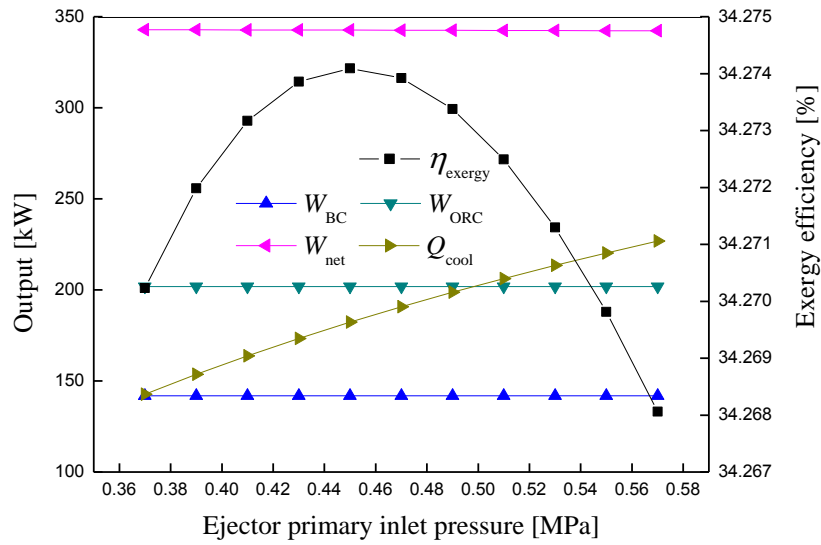
1040   **Fig. 14.** Influences of ejector primary inlet pressure on the output and the exergy

1041   efficiency of the system.

1042

1043   **Fig. 15.** Influences of ejector primary inlet pressure on the levelized exergy cost and

1044   the system capital cost of the system.